Chapter 3
Ancient Seep Carbonates: From Outcrop Appearance to Microscopic Petrography

Krzysztof Hryniewicz

3.1 Introduction

Hydrocarbon seeps are localized submarine ecosystems where hydrocarbons discharge from the seabed into the water column. The majority of extant hydrocarbon seeps have been found on continental margins, where sediment degassing takes place above fluid-laden thick sedimentary columns (e.g., Sibuet and Olu 1998; Campbell 2006; Joye 2020). At seeps, hydrocarbon-bearing fluids migrate upward through various conduits toward the shallow subsurface, where they mix with the sulfate-bearing seawater infiltrating sedimentary pore space. Dissolved methane and sulfate enable the microbially mediated anaerobic oxidation of methane (AOM) according to the formula:

$$CH_4 + SO_4^{2-} \rightarrow HCO_3^- + HS^- + H_2O$$

This results in precipitation of methane-derived authigenic carbonates incorporating ^{12}C-enriched methanogenic carbon in the immediate (meter-scale) vicinity of the fluid outlets, usually within sediment or at the sediment-water interface (Ritger et al. 1987; Peckmann and Thiel 2004). In addition to carbonate cementation, seeping methane and dissolved sulfide formed during AOM provide metabolic energy for chemoautotrophic microbes and their chemosymbiotic invertebrate hosts, which frequently form mass accumulations at seeps (Levin 2005).

In line with their recent counterparts, ancient seep deposits typically (i) have restricted spatial and stratigraphic occurrence, often but not always (cf. Kauffman et al. 1996; Landman et al. 2012, this volume; Meehan and Landman 2016) within relatively deep-water facies, (ii) are characterized by extensive cementation by

K. Hryniewicz (✉)
Institute of Paleobiology, Polish Academy of Sciences, Warszawa, Poland
e-mail: krzyszth@twarda.pan.pl

A. Kaim et al. (eds.), *Ancient Hydrocarbon Seeps*, Topics in Geobiology 53,
https://doi.org/10.1007/978-3-031-05623-9_3

carbonate with low $\delta^{13}C$, and (iii) contain seep-endemic invertebrate macrofossils for which chemosymbiosis or close relations to a chemosynthetic food chain can be reliably inferred (e.g., Campbell and Bottjer 1993; Peckmann and Thiel 2004; Campbell 2006; Kiel et al. 2014a). These criteria have been commonly employed as part of a "seep search strategy," resulting in the identification of numerous ancient seep deposits worldwide (e.g., Kelly et al. 1995; Kauffman et al. 1996; Peckmann et al. 1999a, b, 2002, 2003, 2007, 2011; Kelly et al. 2000; Barbieri et al. 2005; Gill et al. 2005; Kiel and Peckmann 2007; Kiel and Peckmann 2008; Hammer et al. 2011; Agirrezabala et al. 2013; Kaim et al. 2013; Kiel et al. 2013; Zwicker et al. 2015; Hryniewicz et al. 2015a, 2016; Smrzka et al. 2017). In this contribution, the term "ancient seep carbonates" is applied to AOM-related carbonates which have been fossilized in marine rock formations and uplifted above sea level, although there are exceptions to this (e.g., Duranti and Mazzini 2005). Seep carbonates exposed on the seabed in localities where methane seepage has ceased, usually of Pleistocene to Holocene age, are not considered ancient seep carbonates in this review.

The base of this chapter relies on two separate data pools: literature describing extant seep carbonates studied on the seabed and that on ancient seep carbonates studied in outcrop. Both sources offer different, yet to a degree, complementary views of seep carbonate deposits. Extant seep carbonates are studied during or shortly after their formation on the seabed before they can be subjected to burial and diagenetic alteration. Consequently, (i) the most accessible fragments of extant seep deposits are either at the surface or shallow subsurface close to the seabed, while deeper parts are less accessible and less easy to study; (ii) they frequently preserve original mineralogies and textures formed due to AOM before the onset of diagenetic alteration. Ancient seep carbonates, on the other hand, (i) are studied mostly in outcrop, which, unless perfectly parallel to the bedding, allow relatively easy access to deeper horizons of the seep deposit while restricting the access to the surface of the deposit and (ii) have long and complex geological history and accumulate later diagenetic mineralogies and textures which have not yet formed in extant seep deposits. Burial diagenesis can alter mineralogy and textures to such an extent that establishing a straightforward relationship between some apparently congeneric textures in extant and ancient seep carbonates may not be possible.

This chapter is a review of the structure and petrography of ancient seep carbonates, from their size and external appearance in outcrop, to microscopic textures observed in thin section. A detailed discussion of geochemistry of seep carbonates is covered elsewhere in this volume (Cochran et al. this volume; Miyajima and Jenkins this volume). However, some consideration of stable carbon and oxygen isotope composition of particular carbonate phases and lipid biomarker contents of seep carbonates were unavoidable.

3.2 Size of Seep Deposits

3.2.1 Extant Seep Deposits

Seep carbonates incorporate part of the carbon released at methane seeps (e.g., Boetius and Suess 2004; Luff et al. 2004; Tsunogai et al. 2010; Römer et al. 2012); therefore, the size of a seep deposit is to a degree a function of the volume of methane that reached the sediment surface and was metabolized by AOM (Campbell 2006). The largest seep carbonates thus occur in areas where large volumes of methane are delivered to the seabed for prolonged periods of geological time. Some of the largest, single methane seep carbonates known today are up to 180-m-long and 90-m-high carbonate deposits above Hydrate Ridge off Oregon (e.g., Teichert et al. 2005), which started to form over 250 ka and are still growing today, albeit the carbonate accumulation rate was higher during the Pleistocene than afterward (Teichert et al. 2003). Larger seep carbonate deposits such as those at Hydrate Ridge are often supplied by substantial gas migration pathways including active faults (Carson and Screaton 1998) or blow-out pipes associated with mud volcanism (Perez-Garcia et al. 2009; Pape et al. 2014).

The majority of extant seep carbonates are much smaller than those from Hydrate Ridge. For example, at the Nyegga site in the Norwegian Sea where seep carbonates are associated with gas hydrates similar to those from Hydrate Ridge, the largest single carbonate deposit is about 4 m × 3 m × 2 m in size (Hovland and Svensen 2006). Seep carbonate pavements from Monterey Canyon off California are a few square meters in surface or less, and carbonate crusts and pavements measure around 5 cm in thickness (Stakes et al. 1999). Carbonate nodules are most commonly several centimeters in diameter, although larger structures of decimeter scale can form due to the amalgamation of many smaller nodules (Reitner et al. 2005a; Haas et al. 2010). Tubular carbonate conduits are usually either fragmented or partially buried when observed on the seabed; therefore their actual diameters are difficult to ascertain. Fragments of such conduits studied by underwater observation are usually less than 1 m high and up to 0.35 m in diameter (Takeuchi et al. 2007; Magalhães et al. 2012), although larger structures up to 4 m high and 0.5 m in diameter have also been observed (Magalhães et al. 2012). Tubular conduits studied on the seabed have mostly fallen over and are inactive, indicating that a substantial volume of sediment has been removed.

3.2.2 Ancient Seep Deposits

Comparing sizes of extant and ancient seep deposits is innately burdened by uncertainty. This results from the way both occur and are accessed; extant seep carbonates are exposed on the seabed, observed in plan view, and accessed from above using a submersible, with only limited access to deeper parts of the seep system

through gravity coring or drilling. Ancient seep carbonates, on the other hand, are mostly accessed on land in outcrop and are observed in cross section. It is relatively easy to measure the lateral extent of an extant seep carbonate, while measuring its vertical extent is possible only for the parts visible above the seabed or accessed via coring or drilling (e.g., Teichert et al. 2005). Conversely, it is possible to measure the thickness and cross-sectional length of an ancient seep deposit cropping out; however, it is very difficult to measure its lateral extent in all dimensions since these are partially hidden below the ground. An exception to this will be an outcrop surface parallel to the bedding (e.g., Allison et al. 2008), where an ancient seep carbonate can be studied on a plane just like its extant equivalent.

There are a few examples of particularly large ancient seep carbonates that are similar in size compared to the largest extant equivalents. One such example is the Middle Miocene Rocky Knob seep carbonate from East Coast Basin, New Zealand, which is roughly 175 m × 50 m in plan view (Campbell et al. 2008). The Late Triassic (Norian) Graylock Butte 1 (GB1) carbonate from Oregon, USA, measures roughly 70 m in exposed lateral extent and is approx. 4 m thick (Peckmann et al. 2011). A somewhat extreme example, and possibly the largest single seep carbonate preserved, could be a Late Cretaceous (Campanian) seep deposit from Oglala National Grassland, Nebraska, USA, which is ca. 400 m × 200 m in plan view (Fig. 3.1a; Landman et al. this volume, Fig. 14.3f). This deposit has not been studied in detail yet, and it is unknown whether it is a single carbonate body or several smaller ones in close proximity (Andrzej Kaim, personal communication). The Eocene Bear River seep deposit from Washington State, USA, is roughly 68 m long × 38 m wide × 15 m thick (Goedert and Benham 2003). On photographs of the seep deposit from 1954 (Danner 1966: fig. 231), there are fragments of outcrop which are sunken and covered with scree and could very well comprise non-carbonate deposits. The Bear River deposit can thus be several seep carbonate blocks stacked in close proximity, similar to other large ancient seep deposits. The Late Triassic (Norian) Graylock Butte 2 (GB2) deposit from Oregon, USA, represents numerous smaller (meter-scale) carbonate outcrops spread on a ridge along approx. 270 m of strike (Peckmann et al. 2011; own data). The Late Cretaceous Sada Limestone in Shikoku, Japan, comprises numerous meter-scale carbonate bodies dispersed on an area of approx. 250 m × 100 m (Nobuhara 2016). Carbonate stromatolites and boulders forming the Early Jurassic seep carbonate deposit from La Elina, Los Molles Formation, Neuquén Province, Argentina (Gómez-Pérez 2003), are spread in an area roughly 50 m × 45 m × 38 m (Fig. 3.1b, Krzysztof Hryniewicz, own data). Stacking of carbonate blocks forming these deposits implies that before compaction of the host sediment they could have been located much further apart vertically than they are now. Thus, they may be not ideally penecontemporaneous, and at each given time, the size of the seep may have been smaller than the area of the deposit cropping out today.

The great majority of known ancient seep deposits are relatively small carbonate bodies which are meter-scale or smaller and are either loosely scattered over a small

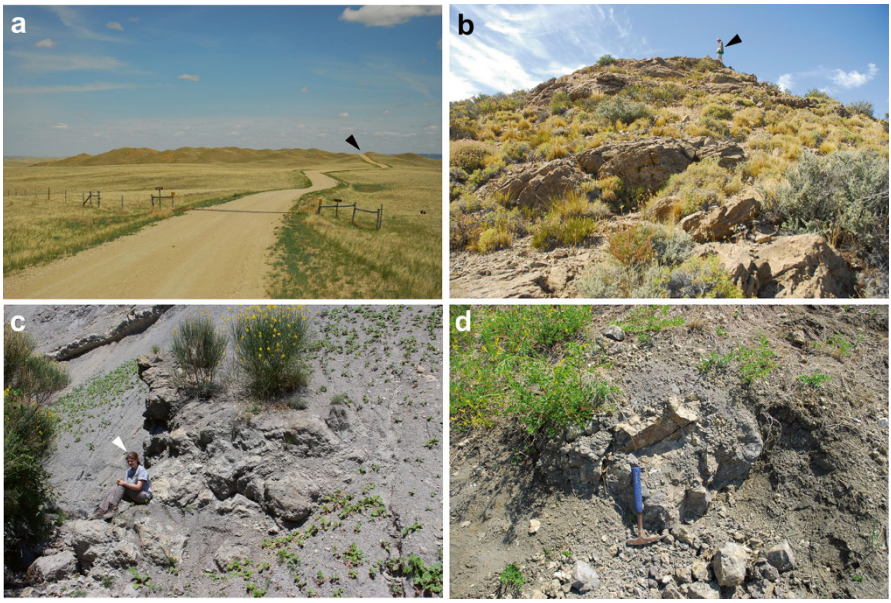

Fig. 3.1 Examples of ancient seep deposits of different sizes. (**a**) Oglala seep deposit (Upper Cretaceous, Campanian), Pierre Shale, Oglala National Grassland, Nebraska, USA. View toward the east. The deposit is ca. 400 m × 200 m in plan view. Montrose Road transecting the deposit in the southern part of the picture for scale (arrowhead). (**b**) La Elina seep deposit, La Elina (Lower Jurassic, Toarcian), Los Molles Formation, Neuquen Province, Argentina (Gómez-Pérez 2003). The deposit is ca. 50 m × 45 m × 38 m in plan view. The person standing on top of the deposit for scale (arrowhead). (**c**) One of the Beauvoisin seep deposits (Upper Jurassic, Oxfordian), Terres Noires Formation, Beauvoisin, Drome, France (Gaillard et al. 1992). Person for scale (arrowhead). (**d**) Small carbonate deposit, Indian Creek seep site (Upper Cretaceous, Campanian), Pierre Shale, Buffalo Gap National Grassland. Hammer for scale

area or isolated in siliciclastic host rock formations (Figs. 3.1c, d and 3.2). For example, the Late Cretaceous (Campanian) seep deposit from Yasukawa, Hokkaido, Japan, comprises four carbonate bodies larger than 0.5 m in diameter spread over an area of few dozen square meters, whereas the remainder of the deposit consists of small-, decimeter-, or centimeter-scale carbonate concretions loosely dispersed in the host sediments (e.g., Jenkins et al. 2007). Various Paleogene and Neogene seep carbonates in the Cascadia margin, Western USA, and Canada are preserved either as small-, decimeter-, or centimeter-sized nodules scattered in the host sediment or as carbonate-filled invertebrate fossils (Nesbitt et al. 2013). An example of a single, small ancient seep carbonate could be an Early Miocene seep carbonate from Tanohama, Tsushima, Japan, which is a lenticular carbonate ca. 3.7 m long and 1 m thick, surrounded by numerous decimeter- to centimeter-sized carbonate concretions scattered in the deep-water mudstone (Hryniewicz et al. 2021).

Fig. 3.2 Examples of smaller ancient seep deposits. (**a**) Yasukawa seep deposit (Upper Cretaceous, Campanian), Omagari Formation, Nakagawa District, Hokkaido, Japan (Jenkins et al. 2007). Two of four larger blocks (ca. 0.5 m in diameter) of seep carbonate (arrowheads) are visible. People in the right side of the picture for scale. (**b**) Tanohama seep deposit (Lower Miocene), Taishu Group, Tanohama, Tsushima, Japan (Hryniewicz et al. 2021). The deposit is ca. 3.7 m long and 1 m thick and is surrounded by numerous smaller, decimeter-sized carbonate nodules. People for scale. (**c**) Eagle Creek seep deposit (Lower Cretaceous, Barremian), Budden Canyon Formation, California, USA (Jenkins et al. 2013). One of the carbonate bodies (ca. 1 m in length) forming the carbonate deposit. Hammer for scale. (**d**) Tanami seep carbonate (upper Eocene–lower Oligocene), Tanamigawa Formation, Tanami, Wakayama Prefecture, Honshu, Japan. The deposit is ca. 3.5–4.5 m × 0.2–0.6 m × 0.2–0.6 m (Amano et al. 2013). Hammer for scale

3.3 Macroscopic Appearance

3.3.1 Extant Seep Carbonates

A characteristic feature of many extant seep carbonates is that their formation occurs at the sediment-water interface (e.g., Stakes et al. 1999; Peckmann et al. 2001; Greinert et al. 2001; Pierre and Fouquet 2007). The process behind this is the dependence of AOM on anaerobic conditions and the presence of dissolved seawater sulfate (Boetius et al. 2000), which results in carbonate formation in the shallow subsurface where the necessary conditions are met. Aerobic methane oxidation, on the other hand, will cause carbonate dissolution (Himmler et al. 2011). This means that most seep carbonates will form close to or at the sediment-water interface in a roughly horizontally oriented zone parallel to it and initially will not protrude significantly either above or below the seabed (Luff et al. 2004). The morphology that

seep carbonates exhibit during early stages of their formation is variable to some extent, but the most commonly reported examples are nodules, pavements, or small tubular concretions (e.g., Reitner et al. 2005a; Haas et al. 2009; Himmler et al. 2015). These precipitates are accessible to underwater observation only after they become exposed by bottom currents (e.g., Matsumoto 1990; Himmler et al. 2011; O'Reilly et al. 2014) or dislodged by other processes, such as gas hydrate growth underneath the carbonate (e.g., Greinert et al. 2001), mud volcano eruptions (e.g., Vanneste et al. 2012), explosive gas release (e.g., Mazzini et al. 2006), pockmark formation (e.g., Webb et al. 2009), or collapse of carbonate overhangs (Hovland and Judd 2007). Seep carbonates can also form at some depth under the sediment-water interface, but this is reported far less often than its shallower-formed counterparts as it is exposed only exceptionally when larger volumes of sediment are eroded away. Examples of such carbonates are various tubular conduits that form the deeper part of the plumbing system of submarine hydrocarbon seeps and were exposed by contourite or other strong eroding bottom currents (e.g., Takeuchi et al. 2007; Magalhães et al. 2012).

In exceptional cases, seep carbonates can also form above the sediment-water interface. Among such cases are marine anoxic basins with a water column depleted in oxygen, allowing AOM and carbonate formation to take place directly at or above the sediment-water interface. A typical example of seep deposits formed under such conditions are meter-scale columnar carbonates from the deeper waters of the Black Sea, which is totally anoxic below 150 m water depth (Peckmann et al. 2001; Reitner et al. 2005b). Similar mechanisms are responsible for the formation of columnar stromatolites in the Oxygen Minimum Zone off Pakistan in the Indian Ocean (e.g., Himmler et al. 2018).

It has been suggested by Teichert et al. (2005) that particularly strong and localized flux of reduced fluids can cause carbonate formation to build up into oxic bottom waters. An example of such a formation are seep carbonate mounds and pinnacles that project into the water column above the sediment, the so-called chemoherms, as observed on Hydrate Ridge off Oregon (e.g., Teichert et al. 2005). Carbonate authigenesis in such cases requires a thin veneer of an oxic/anoxic interface, provided by, for example, mats of sulfide-oxidizing bacteria (e.g., *Beggiatoa*) around active fluid outlets, such that all reduced and oxidized compounds necessary for AOM are simultaneously available (e.g., Boetius and Suess 2004). Methanogenic chemoherms may share some macroscopic features with carbonate buildups known from "classical" carbonate sedimentology (cf. Monty et al. 1995), such as slope aprons (e.g., Teichert et al. 2003).

3.3.2 Ancient Seep Carbonates

Most ancient seep deposits are more or less isolated carbonate bodies occurring within siliciclastic, deep marine host sediments (Campbell 2006 and references therein). Before extant seep deposits were discovered via submersibles on the

modern seafloor, and in the absence of stable isotopic criteria that identify their fossil counterparts, some carbonate deposits later identified as ancient seeps had been referred to as "reefs" (e.g., Danner 1966) and/or olistoliths (e.g., Ager 1965). The "reef" or other buildup-related origin was usually inferred based on textures superficially similar to these found in ancient reefs and mud mounds (cf. Peckmann et al. 1999a, 2002; Campbell et al. 2002; Hryniewicz et al. 2012; see also Monty et al. (1995) for a review of ancient mud mounds). Stromatactoid cavities and clotted micrites found at seep deposits are especially similar to those known from Paleozoic and Mesozoic deep-water mud mounds (e.g., Flajs et al. 1995) and on first glance could have been taken as circumstantial evidence for a buildup origin. An "olistolith" origin, on the other hand, was most probably proposed based on the assumption that a carbonate deposit with a mass accumulation of fossils could not have formed on an otherwise fossil-poor siliciclastic deep-sea bottom and must have been redeposited from shallow water settings (Ager 1965). In fact, several ancient seep deposits, although originating in a deep-water environment, have formed on a slope and subsequently slumped basinward before their final emplacement and burial (e.g., Berti et al. 1994; Sandy 2010; Kiel et al. 2014a, b), so an "olistolith" interpretation in such cases can be sedimentologically correct.

The relationship between seep deposits and the surrounding sediment is most easily observed on fresh outcrops devoid of vegetation. Such conditions are mostly met in arid deserts where the intensity of weathering and physical erosion is low and the vegetation is scant (e.g., Hryniewicz et al. 2017; Smrzka et al. 2017). In other areas, outcrops of seep deposits are restricted to cliffs, riverside scarps, and road cuts (Fig. 3.3a; Gaillard et al. 1992; Landman et al. 2012; Natalicchio et al. 2015; Zwicker et al. 2015; Meehan and Landman 2016; Hryniewicz et al. 2021; Landman et al. this volume), riverbeds (Fig. 3.3b; Jenkins et al. 2007; Kaim et al. 2013), or wave-cut platforms (Fig. 3.3c; Allison et al. 2008; Agirrezabala 2009; Agirrezabala et al. 2013), where weathered material is removed before it can cover up the seep deposit. Even in these settings, a large part of the seep deposit can be obscured by the accumulation of debris (Fig. 3.1a, b; cf. Hickman 2015) or be completely eroded away in a matter of years (e.g., Kiel 2010: fig. 14.5). Many ancient seep carbonate outcrops are partially covered with vegetation (Fig. 3.2a; Campbell et al. 2008), frequently on slopes where an "in situ" situation cannot be confirmed (Fig. 3.2b, c; Campbell and Bottjer 1993: fig. 9; Campbell et al. 2008) or that are partially flooded by a watercourse and covered by sediment (Fig. 3.1d; Kaim et al. 2009). Some seep deposits are known only from float (Fig. 3.3d) and have not been found "in situ" at all. This is particularly true for ancient seep deposits from Spitsbergen (Svalbard) where outcrops are heavily modified by periglacial processes such as frost wedging and solifluction. Out of 16 latest Jurassic–earliest Cretaceous seep deposits found on Spitsbergen, only two are "in situ," with the remainder having slumped to various degrees either en masse or as fragments (Hryniewicz et al. 2015b). A Paleocene seep deposit from Fossildalen, Spitsbergen, is known exclusively from float found in the riverbed (Fig. 3.3d; Hryniewicz et al. 2016).

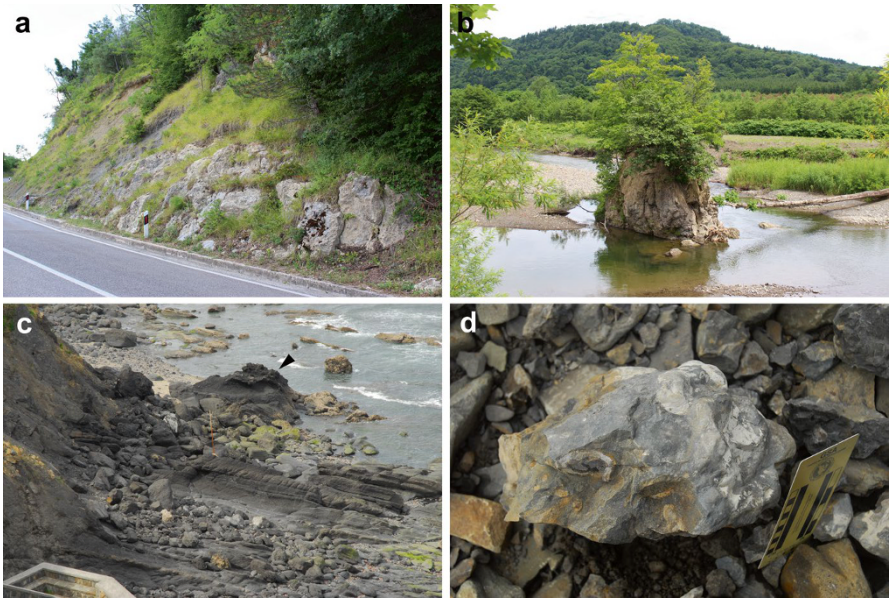

Fig. 3.3 Outcrops of ancient seep deposits. (**a**) Road cut, Buje seep deposit (Eocene), Flysch Units, Istria, Croatia (Natalicchio et al. 2015). The deposit (termed "Buje 1" in Natalicchio et al. 2015) is ca. 4 m thick and extends laterally for ca. 20 m. (**b**) A solitary carbonate islet exposed in a riverbed, Omagari (Upper Cretaceous, Campanian), Abeshinai River, Omagari Formation, Nakagawa District, Hokkaido, Japan. The islet is ca. 10 m in lateral extent. (**c**) Wave-cut platform, Kardala seep deposit (Lower Cretaceous, Albian), Black Flysch Group, Basque Country, Spain. The deposit (arrowhead) is ca. 20 m in lateral extent. (**d**) Float, Fossildalen seep deposit (Paleocene), Basilika Formation, Spitsbergen, Svalbard (Hryniewicz et al. 2016). This particular block is ca. 20 cm along the longer axis

When seep deposits are preserved "in situ," their observed shape can be very variable and can depend on numerous factors, such as the part of the seep deposit cropping out and the intensity and duration of seepage. Portions of the seep deposit formed close to the sediment-water interface frequently occur as lenticular bodies (Fig. 3.4a), which may be arranged parallel to the bedding plane, but not necessarily, and comprise either one larger carbonate body (Smrzka et al. 2017), accumulations of smaller carbonate nodules, or a combination of both (Gaillard et al. 1992; Landman et al. 2012; Meehan and Landman 2016; Hryniewicz et al. 2021). In some cases, only a few loose nodules of ^{13}C-depleted carbonate and associated fauna comprise a seep deposit and are evidence for past seepage activity at a given locality (e.g., Jenkins et al. 2007; Nesbitt et al. 2013). Extensive columnar bodies with the vertical dimension larger than the horizontal, either the so-called pseudobioherms (Fig. 3.4b; Gaillard et al. 1992) or pipe-like structures (e.g., de Beaver et al. 2011), can also form as a result of localized seepage; the latter are likely parts of the subsurface plumbing system of ancient hydrocarbon seeps, together with a variety of tubular concretions (Fig. 3.4c, d; e.g., Pearson et al. 2010; Wiese et al. 2015; Zwicker et al. 2015).

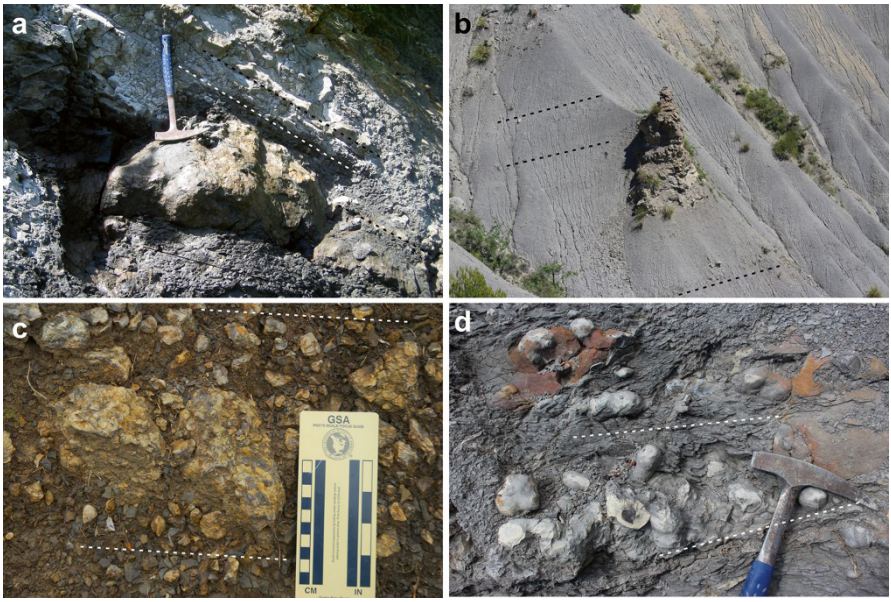

Fig. 3.4 Shapes of ancient seep deposits. (**a**) A lenticular carbonate arranged along the bedding plane (stippled line), Pombetsu seep deposit (Lower Cretaceous, Albian), Yezo Supergroup, Mikasa City, Hokkaido, Japan. (**b**) Pseudobioherm arranged perpendicular to the bedding plane (stippled line), Beauvoisin (Upper Jurassic, Oxfordian), Terres Noires Formation, Beauvoisin, Drome, France (Gaillard et al. 1992). (**c**) Accumulation of nodules and smaller carbonate blocks in the lateral zone of a lenticular seep deposit, stippled line marks the bedding surface, Tanohama seep deposit (Lower Miocene), Taishu Group, Tsushima, Japan. (**d**) Carbonate-filled burrows arranged along and perpendicular to the bedding surface (stippled line); base of one of the pseudobioherms (Upper Jurassic, Oxfordian), Terres Noires Formation, Beauvoisin, Drome, France

The main difficulty in comparing the morphology of ancient seep deposits with their extant counterparts is inferring the relationship of the seep carbonates to the sediment surface. The relationship between the sediment-water interface and the seep carbonates forming presently is verifiable. Conversely, the ancient sediment-water interface changed its position during geological time, and its position in outcrop has to be inferred for the given time based on observed depositional, biological, and diagenetic textures. This indicates that the relationship of the ancient sediment surface to the ancient seep deposit in the outcrop is not obvious or easy to infer, and there are very few diagnostic features indicating that ancient seep carbonates were at any given moment exposed above the seabed. One such feature is the presence of carbonate slope aprons, indicating that carbonate had a positive relief and provided a talus for its surroundings. Such structures are rarely reported from the fossil record; one such example could be cross-bedded slope facies from Miocene seep deposits from New Zealand (Campbell et al. 2008: fig. 13). A further rare case is the Cretaceous Amma Fatma seep deposit from Morocco, where a bed covering a large carbonate body pinches out, likely because the seep carbonate body protruded above the seafloor during the time of its formation (Smrzka et al. 2017). The

presence of fossil epifauna directly attached to the seep carbonate can also be a good proxy that the seep carbonate was exposed above the sediment-water interface. Among such examples are serpulid *Propomatoceros* sp. tubes (Vinn et al. 2014: fig. 5A) and unidentified cementing bivalves (Hryniewicz et al. 2014: fig. 10A, B) attached to fossil carbonate surfaces from the latest Jurassic to the earliest Cretaceous hydrocarbon seep carbonates from Spitsbergen. Many examples of attaching epifaunal fossils are, however, found either dispersed in the carbonate matrix or attached to other fossils (e.g., Vinn et al. 2013; Hryniewicz et al. 2015b); hence, their presence should not always be taken as unambiguous evidence of positive relief of ancient seep deposits.

3.4 Macroscopic Petrography

3.4.1 Extant Seep Carbonates

Macroscopic petrography of extant seep carbonates can be studied either directly on the seabed (e.g., Himmler et al. 2011: fig. 2a–d), on hand samples retrieved from the seabed by submersibles (e.g., Mazzini et al. 2004: fig. 4a, 5a, 6a, 7a, b; Himmler et al. 2011: fig. 2e–f; Smrzka et al. 2019: fig. 3b, d, 4b–d), or on polished slabs of retrieved hand samples (e.g., Mazzini et al. 2004: fig. 3; Teichert et al. 2005: fig. 5b–f; Haas et al. 2010: fig. 2c, 3b, 5b; Himmler et al. 2011: fig. 3). Since seep carbonates are frequently covered with biota or sediment which otherwise obscures the details visible on the surface (e.g., Van Dover et al. 2002: fig. 3a; Webb et al. 2009: fig. 3 b–d, e), observation of retrieved samples is a more unequivocal way to observe macroscopic petrography of extant seep deposits. This is with the proviso that the features targeted do not exceed the size of the sample extracted.

One of the most conspicuous features of the majority of extant seep carbonates is the abundance of cavities, which either show some preferential orientation (e.g., Himmler et al. 2016: fig. 2) or do not (e.g., Himmler et al. 2011: fig. 2, 3). A characteristic type of cavity at seep carbonates is represented by various tubular structures that acted as conduits for fluids and methane (e.g., Hovland 2002; Teichert et al. 2005; Haas et al. 2010; Malaghães et al. 2012). The cavities may remain unlined or be lined with cements to various degrees (e.g., Teichert et al. 2005; Himmler et al. 2011). There are multiple origins of cavities within the seep deposit, such as carbonate dissolution during periods of elevated acidity (Himmler et al. 2011), occlusion of cavities in between centers of carbonate precipitation (e.g., Haas et al. 2010), or dissolution of gas hydrate enclaves enclosed within carbonate precipitates (e.g., Greinert et al. 2001). Gas hydrates at seeps are frequently associated with breccias which formed from relatively brittle carbonate (Bohrmann et al. 1998); this is likely because formation of gas hydrate involves a significant volume increase and this has a potential for disrupting even strongly cemented layers of carbonate. Reasons for brecciation can be multiple and involve, for example, cementation of soft sediment brecciated due to mud and fluid expulsion (Vanneste et al.

2012) or slumping and collapse of positive carbonate relief (Greinert et al. 2001; Teichert et al. 2005). Different generations of breccias at extant seeps form at the surface or below it (cf. Greinert et al. 2001), and only the former are generally available for submersible-borne observation and sampling.

Laminated fabrics comparable to those known from other depositional environments also occur at seeps (e.g., Greinert et al. 2002; Himmler et al. 2018). The exact origin of the lamination in seep carbonates is difficult to ascertain as there are multiple causes for lamination in sedimentary rocks. At seeps, particular laminae grow toward the source of reducing compounds and generally into the sediment where the fluid flow originates, thus conforming to a general pattern of downward growth of seep deposits (e.g., Greinert et al. 2002). However, when bottom waters are oxygen-deficient and allow for an upward growth of seep carbonate, laminations can also form from the sediment surface upward into the water column similar to the cases known from more "classical" depositional settings (Himmler et al. 2016). Sediment baffling and trapping by chemosynthetic microbial mats can be one of the causes for laminated fabrics in seep carbonates (Himmler et al. 2016); microbial mats, in general, may become permineralized by Mg calcite and aragonite precipitates (Reitner et al. 2005b), and sediment baffling may even further contribute to the expression of particular laminae. Cementation of sedimentary laminations accentuated by gas hydrate can also result in layered carbonates (Mazzini et al. 2004). Fillings of tubular conduits (e.g., Greinert et al. 2002: fig. 4) and concretions forming at seeps are frequently layered in appearance (e.g., Reitner et al. 2005a; Haas et al. 2010).

One of the more peculiar fabrics of seep deposits are carbonate spheres formed due to calcification of microbial mats around fluid outlets (Reitner et al. 2005b). Amalgamation of such cemented microbial spheres results in thrombolitic fabric superficially similar to that known from non-seep fossil microbial carbonates (cf. Shapiro 2000). An important aspect of seep carbonate formation is biogeochemical feedback affecting rates of fluid flow, AOM, and carbonate precipitation (cf. Luff et al. 2005); thus, very complex patterns involving cavities, nodules, lamination, layering, and zonation will form at seeps due to self-regulatory processes even without any external cause.

3.4.2 Ancient Seep Carbonates

In addition to polished slabs used to study extant seep deposits recovered from the seabed, exposed surfaces are a very valuable source of information. This is largely due to subaerial weathering that accentuates even slight differences in mineralogy, crystal size, clay admixture, or fossil content that would otherwise be difficult to observe with the naked eye on unweathered surfaces. Some of the more spectacular examples of such features are, for example, carbonates with ankerite-filled vesicomyid bivalve shells (red-weathering) "floating" in a calcitic matrix (beige-weathering) from Early Miocene seep deposits from Tsushima, Japan (Fig. 3.5a; Hryniewicz et al. 2021: fig. 6), and tubeworm facies in Devonian (Peckmann et al. 2005: fig. 3),

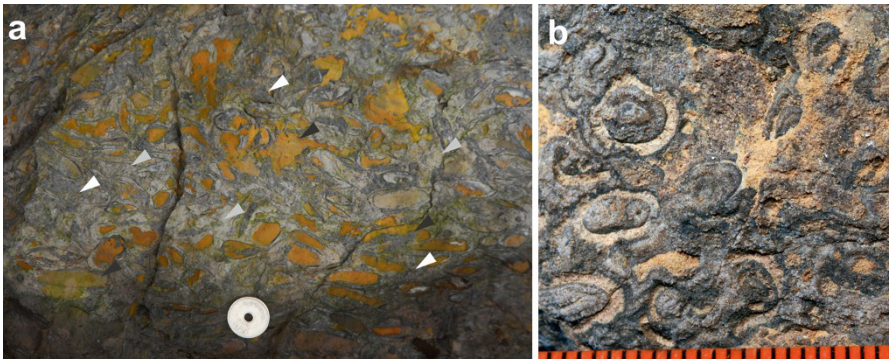

Fig. 3.5 Macroscopic petrography of ancient seep carbonates. (**a**) Weathering-accentuated differences in mineralogy; ankerite-filled vesicomyid bivalves and cavities (orange, indicated by black arrowheads) contrast with grey cements (indicated by white arrowheads) and beige microcrystalline carbonates (grey arrowheads). Kanoura seep deposit (Lower Miocene), Taishu Group, Tsushima, Japan (Hryniewicz et al. 2021). Coin for scale. (**b**) Weathering-accentuated agglutinated tubeworms within microcrystalline carbonate from La Elina seep deposit (Lower Jurassic, Toarcian), Los Molles Formation, Neuquen Province, Argentina (Gómez-Pérez 2003). Scale in mm

Jurassic (Fig. 5B; Gómez-Pérez 2003: fig. 8a), Cretaceous (Hikida et al. 2003: fig. 3), and Oligocene (Goedert et al. 2000: fig. 3) seep deposits. Various breccias, either polymictic or monomictic (e.g., Hikida et al. 2003: fig. 3.2, Bojanowski 2007; Conti and Fontana 2007; Conti et al. 2007), are also clearly visible on exposed surfaces, again due to differential weathering of clasts and matrix.

The macroscopic textures known from ancient seep deposits are roughly similar to those known from their extant counterparts (Figs. 3.6 and 3.7), with a few exceptions due to biological or geological causes. Breccias (Fig. 3.8) occur in both ancient and extant seeps, although perhaps not as commonly in ancient seep carbonates as in their *recent* counterparts. Reasons for ancient seep brecciation have been traditionally linked with gas hydrate buildup and dissociation (Bojanowski 2007; Conti and Fontana 2007) or dissipation of fluid overpressure (Hryniewicz et al. 2012). Hydrate-related brecciation may be evidenced by angular voids filled with cements "floating" within microcrystalline carbonate; this texture could represent a relic of hydrate clasts occluded with cements during or after hydrate dissociation (Bojanowski 2007).

Ancient seep textures different from those known from extant seeps may result, for example, from different faunas living at seeps during the geological past than are living in such environments today. Perhaps the most spectacular example of such biota are seep-dwelling brachiopods, which occur in Silurian–Cretaceous seeps in mass accumulations of numerous stacked individuals (e.g., Campbell and Bottjer 1995; Peckmann et al. 2001, 2007, 2011; Sandy 2010; Kiel et al. 2014a; Jakubowicz et al. 2017). The brachiopod carbonates (Fig. 3.9) from ancient seeps are unique due to (i) ecology of ancient seep-dwelling brachiopods, which were adapted to live epifaunally in low flux conditions, where no comparable shelly epifauna live today (cf. Sahling

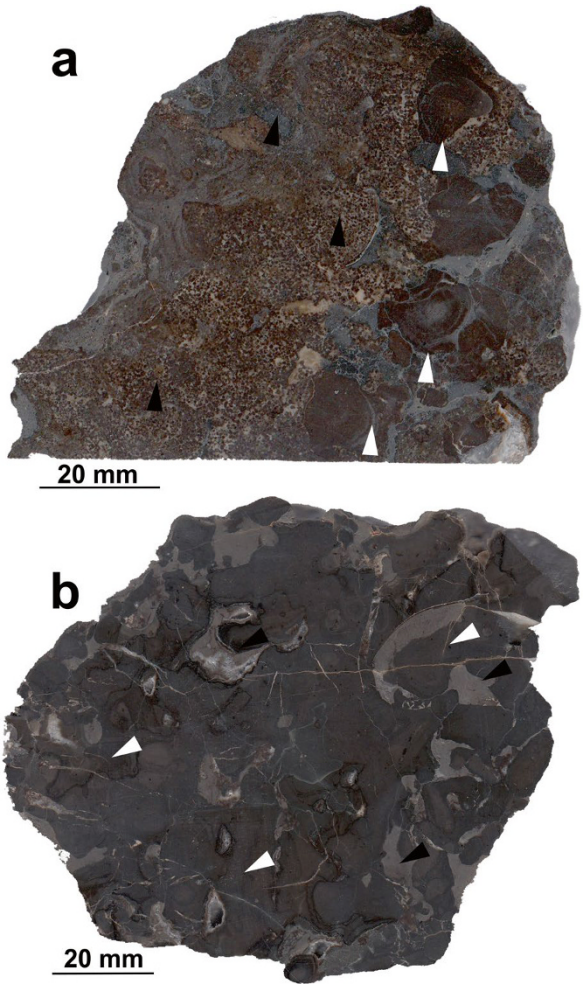

Fig. 3.6 Macroscopic petrography of ancient seep carbonates. (**a**) Microcrystalline carbonate nodules (white arrowheads) next to peloidal carbonate (black arrowheads). Baška seep deposit (Lower Cretaceous, Barremian), Hradiště Formation, Carpathians, Czech Republic (Kaim et al. 2013). (**b**) Coalesced microcrystalline carbonate nodules (white arrowheads) enclosing ambient deep-sea marly sediment (black arrowheads). Beauvoisin (Upper Jurassic, Oxfordian), Terres Noires Formation, Beauvoisin, Drome, France (Gaillard et al. 1992)

et al. 2002), and (ii) calcitic shells of brachiopods, which are much more chemically resistant than aragonitic or mixed aragonitic-calcitic shells of seep bivalves and much more frequently preserved in large numbers. Brachiopod shell frameworks filled with micritic carbonate are hallmarks of several ancient seep deposits and have no equivalent in extant seep carbonates. Rock-forming accumulations of ammonites in Late Cretaceous-aged seep deposits from Western Interior Seaway, USA, are also without equivalent at extant seeps (Landman et al. 2012, this volume).

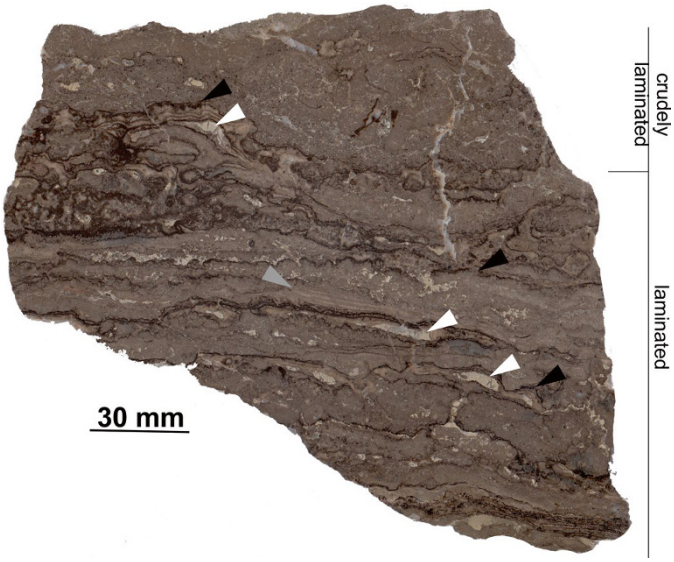

Fig. 3.7 Macroscopic petrography of ancient seep carbonates. A block of limestone showing juxtaposed laminated and crudely laminated facies; laminated facies is composed of layered sediment (sedimentary onlap indicated by grey arrowhead) and pyrite-covered corrosion surfaces (black arrowheads); white arrowheads indicate possible keystone vugs. Paskenta (Upper Jurassic, Tithonian), Great Valley Group, California, USA (Campbell et al. 2002)

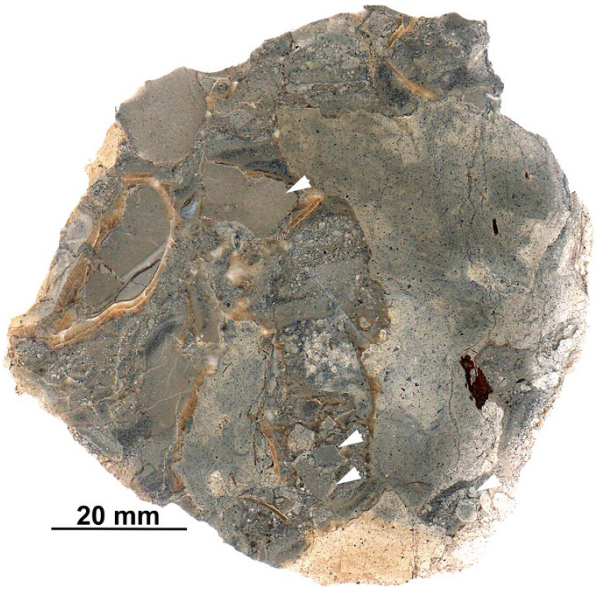

Fig. 3.8 Microcrystalline carbonate and banded cements juxtaposed with pocket of breccia; note angular clasts with lithology similar to that of the surrounding carbonate, indicating little transport (arrowheads). Kami-Atsunai (Oligocene), Nuibetsu Formation, Tokachi District, Hokkaido, Japan

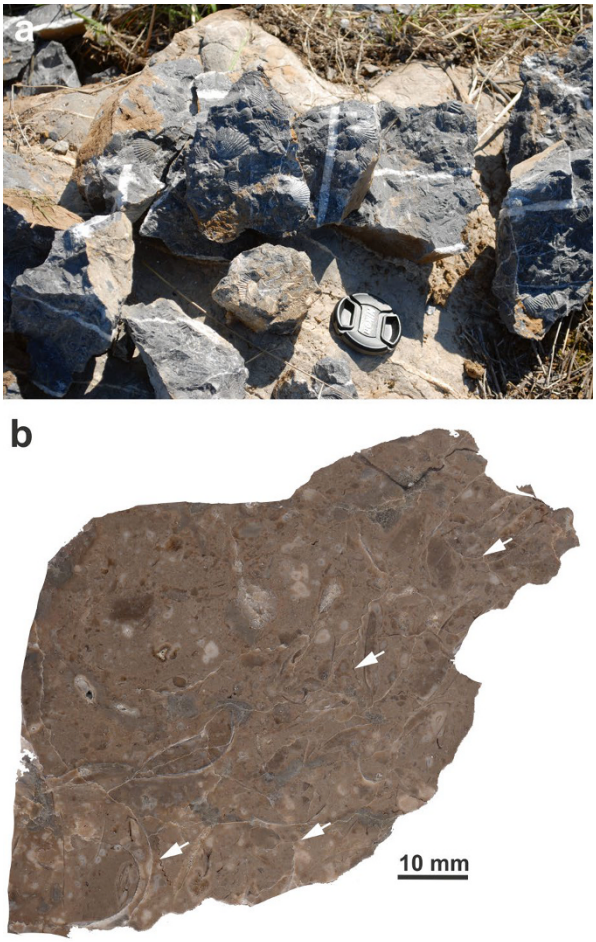

Fig. 3.9 Macroscopic petrography of ancient seep carbonates. (**a**) Rock-forming accumulation of dimerelloid brachiopod *Anarhynchia gabbi*, Bedford Canyon seep deposit (Middle Jurassic), Bedford Canyon Formation, California, USA. Lens cap for scale. (**b**) A polished slab of brachiopod carbonate with numerous thin brachiopod shells (arrows), Rice Valley (Lower Cretaceous, Hauterivian), Great Valley Group, California, USA

The long geological history of some ancient seep carbonates ensures that, in contrast to their extant counterparts, some ancient seep carbonates have been subjected to a much longer and more complex diagenesis in shallow and deep subsurface. Thus, during their diagenetic history, ancient seep carbonates accumulated textures which have not yet formed in extant seep carbonates (e.g., Campbell et al. 2002; Agirrezabala 2009). For example, cavities that are typical for extant seep carbonates are occluded in ancient seep deposits with one or several generations of fillings comprising clastics, carbonates, sulfate or quartz precipitates, or pyrobitumens (e.g., Campbell et al. 2002; Agirrezabala 2009; Hryniewicz et al. 2021). This is true for most ancient seep deposits, and only in some cases have the cavities so

typical of extant seep deposits escaped occlusion (e.g., Hryniewicz et al. 2015a: 234). Mineral phases and their spatial relationships can be observed rather easily on polished slabs and provide a first, approximate estimate of the geological history of a particular seep deposit. A more detailed study of petrography has to be undertaken using microscopic tools.

3.5 Microscopic Petrography

3.5.1 Extant Seep Carbonates

The phases formed at seeps due to AOM occur in close proximity or in superposition, often in mm or cm scale (e.g., Luff et al. 2004, 2005). It may be thus difficult to differentiate them without microscopic techniques, such as transmitted and reflected light and scanning electron microscope (SEM) imaging, aided by fluorescence microscopy for illustration of additional features (e.g., Aloisi et al. 2000; Pierre and Fouquet 2007; Feng et al. 2008, 2010; Himmler et al. 2018; Zwicker et al. 2020). Also, the broad range of chemical conditions found at seep environments causes different minerals to form in spatial or temporal succession, including not only aragonite, Mg calcite, and dolomite but also sulfates (barite), sulfides (pyrite), and phosphates. The identification of mineral (especially carbonate) phases may be equivocal using optical methods alone and requires other techniques, such as X-ray diffraction (e.g., Greinert et al. 2002; Mazzini et al. 2005). Even when phases can be differentiated using the above-mentioned methods, assigning them to a particular environment is very difficult using optical features alone. This is because the same mineral forming different phases can vary considerably with respect to environment-diagnostic stable $\delta^{13}C$ and $\delta^{18}O$ signatures; Sr, Mg, or REE elements; or lipid biomarker content (e.g., Leefmann et al. 2008; Feng et al. 2008, 2010; Zwicker et al. 2018). Hence, geochemical investigations are an inherent part of the microscopic petrographic studies of extant seep deposits.

To fully review all microscopic phases known from extant seep deposits is beyond the scope of this chapter. Given the amount of information presented in combined microscopic and geochemical studies of extant seep carbonates, it would perhaps require a separate volume. However, some phases are the most typical of seep carbonates. In this chapter, their appearance, origin, and significance are briefly discussed, with reference to the literature on the subject.

Two mineral phases are especially well documented in extant seep deposits: microcrystalline carbonates and banded carbonate cements. The proportion of both phases varies between different seep deposits, but together they are the volumetrically dominant mineral phases that comprise the bulk of most seep carbonates.

Microcrystalline carbonate at seeps can be composed of aragonite, Mg calcite, low-Mg calcite, or dolomite (e.g., Jørgensen 1989; Reitner et al. 2005a; Haas et al. 2010). Both micrite-sized (<4μm) and microspar-sized crystals (between 5μm and 30μm) occur. Aragonite and calcite mineralogies form close to the sediment-water

interface where carbonate anions (HCO_3^{2-}) provided by AOM and Ca^{2+} diffusing downward from seawater are available (Luff et al. 2005). Another control on seep carbonate mineralogy is the concentration of seawater sulfate anions (SO_4^{2-}), which inhibit magnesium partitioning into calcite, thus favoring aragonite formation when communication between seawater and pore space is maintained. Since aragonite forms much faster than calcite (Luff and Wallmann 2003), conditions in higher flux areas favor aragonite over calcite precipitation. Conversely, dissolved sulfide catalyzes Mg dehydration, thus enabling Mg calcite precipitation (Smrzka et al. 2021). As the alkalinity decreases due to decreasing flux, sediment deposition on the seabed, or clogging the pore space with carbonate, precipitation of aragonite slows down, and that of calcite "catches up," causing the latter to gain in importance. In addition, recrystallization of aragonite to calcite takes place, also resulting in the formation of calcitic microcrystalline carbonates.

The substrate for carbonate precipitation at seeps may be clasts or aragonite shells, which become covered with aragonite crusts (e.g., Aloisi et al. 2000: fig. 3a). Both aragonite and calcite also precipitate directly within the organic sheets as dumbbell-shaped aggregates and spherulites that nucleate on matrices of extracellular polymeric substances (e.g., Reitner et al. 2005a, b). At seeps, microbial substrates are extremely important for carbonate authigenesis; however substrates derived from, for example, sponges can also occur (cf. Dupraz et al. 2009). Organomineralization at seeps results in such fabrics as, for example, cemented microbial bundles or filaments, mineralized extracellular polymeric substances (e.g., Himmler et al. 2018: fig. 3), and peloids or clotted micrites of possible microbial origin (e.g., Teichert et al. 2005: Fig. 7c; Feng et al. 2010: fig. 4; cf. Flügel 2004 for a review of peloid origin). These fabrics are to a large degree similar to fabrics known from microbial carbonates forming elsewhere, for example, in cryptic habitats within reefs, hot springs, hypersaline ponds, or shallow water settings (e.g., Riding and Awramik 2000; Dupraz et al. 2009; Diaz and Eberli 2022). However, seep carbonates contain ^{13}C-depleted lipid biomarkers characteristic for AOM-mediating microbial consortia (methane-oxidizing archaea and sulfate-reducing bacteria; Boetius et al. 2000), and these are exclusive to such environments.

The formation of dolomite at seeps is somewhat less well constrained than that of aragonite and calcite. Previous studies suggested that sedimentary dolomite may form close to the area where sulfate is being consumed and the decomposition of an aqueous $MgSO_4^0$ complex takes place, followed by a rise in the Mg/Ca ratio (Baker and Kastner 1981). More recent studies somewhat corroborate this view (Lu et al. 2018). Sulfate reduction due to AOM and migration of released Mg ions to the parts of the seep system where little sulfate is available generally favors dolomite precipitation in the deeper subsurface (e.g., Takeuchi et al. 2007; Tong et al. 2019).

Botryoidal carbonate cements form due to rapid precipitation from supersaturated solutions. Either aragonite or calcite can precipitate and form botryoid crystal aggregates, depending on alkalinity, water temperature, and mineralogy of the substrate (cf. Aissaoui 1985, 1988; Savard et al. 1996). While this type of cementation is common at hydrocarbon seeps, it is not exclusive to them and occurs wherever supersaturated solutions are flushed through sedimentary pore space, for example,

on submerged reef slopes (Grammer et al. 1993). Aragonite and calcite forming botryoids are best distinguished with X-ray diffraction of powdered samples and staining with Feigl's solution. However, preliminary optical identification can be done under optical microscopy using normal and cross-polarized light; aragonite botryoids are composed of fine, flat-topped crystallites, while in calcite botryoids, each crystallite has a pyramid-shaped angular termination (Ross 1991).

Botryoidal cements form rather rapidly and require a large volume of fluids pumped through the pore space in a short time. Thus, at seeps they are associated with those parts of the seep system with a high flux of alkaline fluids. Such areas can be fluid conduits and outlets (e.g., Teichert et al. 2005), a matrix of carbonate breccia, often in the vicinity of dissociating methane hydrates (e.g., Greinert et al. 2001), and worm tubes (e.g., Haas et al. 2009). Botryoidal cements, either calcite or aragonite, can form several layers separated by pyrite crusts, indicating recurrent episodes of carbonate cementation and dissolution (own data).

Botryoidal aragonite is heavily depleted in ^{13}C, but it does not contain any meaningful concentrations of AOM-specific biomarkers (e.g., Himmler et al. 2015). This is likely because AOM took place elsewhere and alkalinity was not produced directly where the botryoidal aragonite precipitated (Hagemann et al. 2013). Instead, the carbonate phase which forms in direct proximity with AOM is termed "whitish aragonite." This phase contains the largest concentration of ^{13}C-depleted biomarkers such as archaeol, *sn*-2-hydroxyarchaeol, crocetane, PMI, and DAGE typical for AOM-mediating microbial consortia (Leefmann et al. 2008).

Among the non-carbonate minerals occurring at seeps, pyrite (FeS_2) is one of the more common ones. Mechanisms of pyrite precipitation at seeps are based on iron and organoclastic sulfate reduction taking place in organic-rich marine sediments, as well as AOM-related formation of sulfide (Peckmann and Thiel 2004; Cochran et al. this volume). These provide conditions for the formation of amorphous iron sulfides and greigite (Fe_2S_4), which transform into more stable pyrite. During seepage, excess sulfide is produced continuously through AOM, and pyrite precipitation at seeps is limited largely by the availability of sedimentary iron rather than sulfide. Thus, seeps developed in areas with little reactive iron are devoid of pyrite (e.g., Aloisi et al. 2000; Himmler et al. 2011). Pyrite at seeps can occur as framboidal aggregates dispersed in the carbonate matrix or filling pores (e.g., Feng et al. 2008) or as coatings on corrosion surfaces, which form during dissolution of authigenic carbonate by acidic solutions. The relation between pyrite formation and carbonate dissolution is not clear, however. Pyrite precipitation has been suggested (Peckmann and Thiel 2004) to take place when reduced iron and sulfide react, causing acidification of the environment according to the idealized reaction:

$$Fe^{2+} + 2H_2S \rightarrow FeS_2 + 4H^+$$

However, corrosion surfaces without any pyrite incrustation form in seeps as well due to sulfide oxidation and resulting formation of sulfuric acid (Himmler et al. 2011):

$$H_2S + 2O_2 \rightarrow SO_4^{2-} + 2H^+$$

Thus, pyrite incrustation of corrosion surfaces within seep carbonates can be either a phenomenon synchronous with corrosion or post-dating it.

3.5.2 Ancient Seep Carbonates

Techniques used to study extant and ancient seep carbonates are similar. Observations of carbonate thin sections under transmitted light and polished or etched surfaces under SEM are standard methods allowing observation and identification of phases (e.g., Peckmann et al. 2002; Peckmann and Thiel 2004; Barbieri and Cavalazzi 2005; Barbieri et al. 2005). In addition, techniques like epifluorescence microscopy and cathodoluminescence imaging are used (e.g., Buggisch and Krumm 2005; Hammer et al. 2011; Amano et al. 2013; Agirrezabala et al. 2013; Little et al. 2015; Natalicchio et al. 2015; Zwicker et al. 2015, 2018; Hryniewicz et al. 2021) as they can capture early authigenic phases which are otherwise modified because of later overprint.

One of the differences in studies of extant and ancient seep carbonates is that while the former are a mixture of aragonite and calcite, the latter are dominantly calcite and aragonite is rarely preserved. This is because aragonite is less stable during carbonate diagenesis than calcite (cf. Luff et al. 2005) and is preserved only under conditions of a relatively closed system with limited mobilization of elements (cf. Zwicker et al. 2018). This applies to all phases building ancient seep deposits.

Another difference lies in the paragenetic sequence of ancient seep carbonates, which are composed of two genetic components: the early diagenetic and late diagenetic (e.g., Campbell et al. 2002; Agirrezabala 2009; Blouet et al. 2017; Zwicker et al. 2018). The distinction between those two components is based on the environment of formation (at or close to the seabed for early diagenetic vs. in burial for late diagenetic), as well as thermal (ambient or near-ambient seawater temperature vs. elevated burial temperatures) and distribution criteria (broad vs. pore filing) (Agirrezabala 2009). The early diagenetic components of ancient seep deposits are a close equivalent to extant authigenic carbonates which form at present-day seeps, with a proviso that not all early diagenetic phases in ancient seep carbonates are recognized as authigenic phases in extant seep carbonates. This is because (i) some ancient early diagenetic phases apparently formed in shallow subsurface and thus are hardly accessible for sampling by submersibles at extant seeps and (ii) authigenic aragonite building the bulk of extant seep deposits is rarely preserved in the fossil record as outlined above; hence, its dissolution and recrystallization will result in a proportional increase in the significance of calcite in ancient seep carbonates. An example of the sampling bias may be siliceous cements, which formed after microcrystalline carbonate and banded cements, yet in the shallow subsurface when the fluid flux was still active (cf. Smrzka et al. 2015). The importance of aragonite

dissolution in terms of the appearance of some carbonate phases in ancient seep carbonates has been outlined elsewhere in this contribution.

The early diagenetic microcrystalline carbonates and banded cements at extant and ancient seep carbonates are similar. One to several generations of microcrystalline carbonates can be recognized based on their texture (Fig. 3.10a), $\delta^{13}C$ and $\delta^{18}O$ signatures, or elemental composition (e.g., Zwicker et al. 2015, 2018). Usually, the first generation of microcrystalline carbonate (Fig. 3.10a, b), termed micritic matrix, micrite 1, or otherwise, is volumetrically dominant and the most ^{13}C-depleted of all micrites, indicating formation influenced by AOM (Campbell et al. 2002; Agirrezabala 2009; Blouet et al. 2017). Later microcrystalline carbonates formed during early diagenesis, for example, pipe-filling micrites formed deeper in the sediment, tend to have much higher $\delta^{13}C$ signatures than the remainder of the conduits, indicating formation from a different carbon pool, for example, one affected by methanogenesis rather than by AOM (Zwicker et al. 2015). Such later phases, either micrite or microsparite, can be volumetrically important components of carbonate-cemented tubular conduits (e.g., Wiese et al. 2015; Zwicker et al. 2015; Blouet et al. 2017).

Banded cements (Fig. 3.10c–e) of ancient seep deposits are now largely recrystallized to calcite, but initial mineralogy may be indicated by crystal morphology, providing this was not modified during recrystallization. Initial aragonite can be identified by its flat-topped, needle-shaped crystals (Fig. 3.10c; Savard et al. 1996; Kiel et al. 2014a, b; Hryniewicz et al. 2016, 2021). In most cases, closer examination reveals that initial aragonite has been replaced by calcite pseudospar, which can be identified by randomly oriented optical crystal axes (Fig. 3.10d, e; cf. Ross 1991: fig. 5), and confirmed by X-ray diffraction (e.g., Hryniewicz et al. 2021). Original calcite mineralogy of banded cements can be identified due to pyramidal crystal tops and sweeping light extinction (e.g., Hammer et al. 2011: fig. 4f; cf. Ross 1991). Banded cements are one of the earliest phases of ancient seep deposits, forming after the first microcrystalline carbonate has cemented the pore space (e.g., Campbell et al. 2002; Hryniewicz et al. 2012). Ancient banded cements are frequently found in proximity to the so-called yellow cements (Fig. 3.10c–e). These cements are equivalent to the "whitish aragonite" of Leefmann et al. (2008), but they preserve aragonitic microcrystalline texture only in exceptional cases (Zwicker et al. 2018 and references therein) and otherwise are recrystallized to calcitic, yellow coarse spar (e.g., Hammer et al. 2011; Hryniewicz et al. 2021). Strong fluorescence of yellow cements (Zwicker et al. 2018) and very high contents of biomarkers typical for AOM-mediating microbial consortia (Hagemann et al. 2013) indicate that the phase originated through permineralization of microbial communities mediating AOM and causing the rise of alkalinity at seeps. Banded and yellow cement associations sometimes form "cake"-like textures, with several layers of yellow and banded cements superimposed, indicating recurrent growth and cementation of AOM-mediating microbial consortia.

Because ancient seep carbonates formed close to or at the sediment-water interface, they may have become exposed and modified by bottom currents just as "regular" marine carbonates do. Textures formed during these processes indicate that the

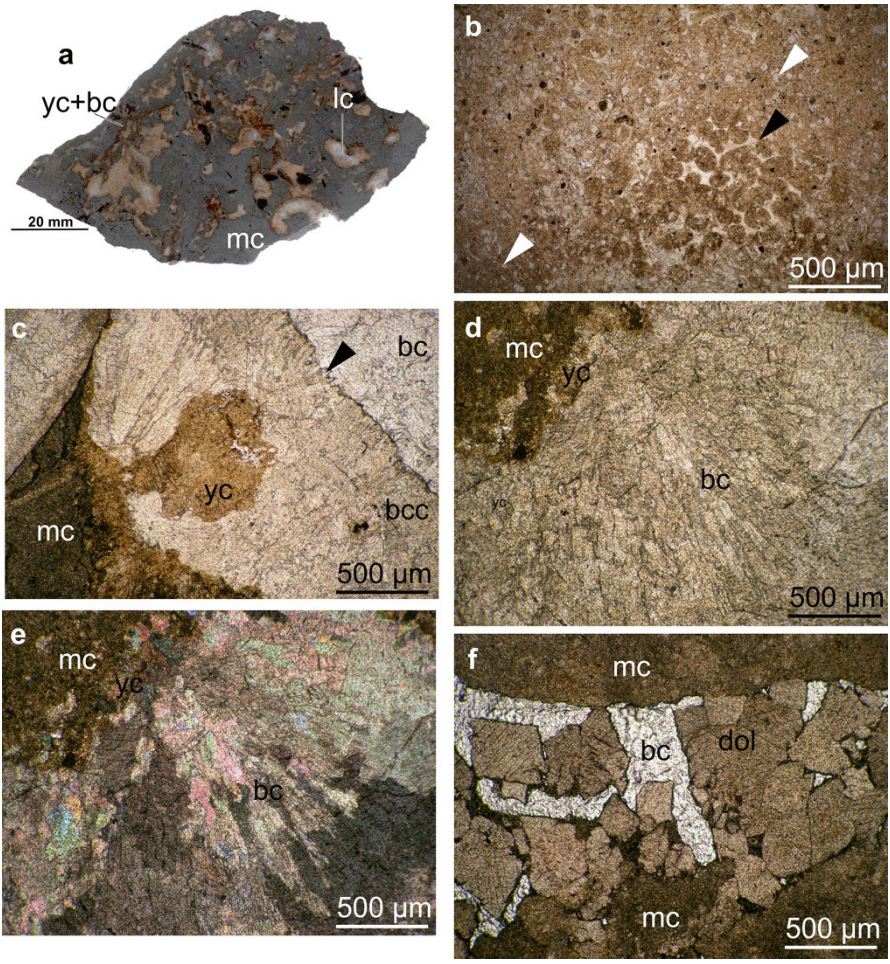

Fig. 3.10 Microscopic petrography of ancient seep carbonates. (**a**) An example of spatial distribution of main textures in ancient seep carbonate polished slab. bc, banded cement; lc, late cements; mc, microcrystalline carbonate; yc, yellow cements. Shikorozawa seep deposit (Lower Cretaceous, Albian), Yezo Supergroup, Hokkaido, Japan. (**b**) An example of microcrystalline carbonate cementing quartz grains (white arrowheads) and fecal pellets (black arrowhead). Fossildalen seep deposit (Paleocene), Basilika Formation, Spitsbergen, Svalbard (Hryniewicz et al. 2016). Plane-polarized light. (**c**) An example of an association of microcrystalline carbonate and cavity-filling yellow and banded cements, with flat-topped crystal termination (arrowhead). The remainder of the cavity is filled with blocky calcite. bc, blocky calcite; bcc, banded cements; yc, yellow cements; mc, microcrystalline carbonate. Tanohama seep deposit (Lower Miocene), Taishu Group, Tsushima, Japan (Hryniewicz et al. 2021). Plane-polarized light. (**d**) An example of cavity-filling yellow-banded cement association. (**e**) The same sample, with cross-polarized light. Note randomly oriented crystal optic axes. Both D and E from Tanohama seep deposit (Lower Miocene), Taishu Group, Tsushima, Japan (Hryniewicz et al. 2021). (**e**) An example of late diagenetic filling of cavity within early microcrystalline carbonate. The late diagenetic filling is composed of blocky calcite and dolomite crystals. bc, blocky calcite; dol, dolomite; mc, microcrystalline carbonate. Tanohama seep deposit (Lower Miocene), Taishu Group, Tsushima, Japan (Hryniewicz et al. 2021). Plane-polarized light

carbonate was exposed at a certain time and are good proxies of ambient conditions at the site of seepage. For example, sediment transported by submarine currents over the seep carbonate may have entered the cavity where a particular banded cement precipitated and formed a pocket incorporated into the cement crust, as illustrated for Paleocene seep carbonates from Spitsbergen (e.g., Hryniewicz et al. 2016: fig. 6E). Bottom currents may also have remodeled shell debris of seep-dwelling biota. In one of the earliest Cretaceous seeps from Spitsbergen, concentration and local imbrication of shells (i.e., orientation of elongated clasts so that they overlap each other) were caused by submarine currents removing finer particles from the surface of the seep deposit. Early diagenetic carbonates can bear signs of erosion, transport, and subsequent redeposition. For example, some seep carbonate-filled thyasirid bivalves from the Paleocene shallow water succession of Spitsbergen are found within the "normal" marine siltstone. Yellow and banded authigenic cements filling cavities within these fossils have been displaced from their original position, fragmented, and incorporated into classic filling of the remaining cavity (Hryniewicz et al. 2016: fig. 6A–D). This has been interpreted as an effect of redeposition at the seep where carbonate authigenesis took place through mass movement down the shallow marine delta slope. The crusts were fragmented during transport, and the remainder of the cavity was filled after the redeposited shell had been covered with sediment.

Silicification is an important early diagenetic process which has shaped several ancient seep carbonates. It was especially important in those environments where radiolarian and diatom tests were common as sources of biogenic silica (Kuechler et al. 2012; Smrzka et al. 2015; Miyajima et al. 2016). The mobilization of silica at seeps is possible due to AOM-related rise of alkalinity, with CO_2 degassing due to seepage amplifying the effect on pH increase and dissolution of siliceous tests (Smrzka et al. 2015). Migrating silica is re-precipitated at the periphery of a seep deposit where the alkalinity and rate of AOM are lower than near the center of the seep or after a decrease in pH (e.g., due to sulfide oxidation or due to cessation of AOM) causing supersaturation with respect to silica. The latter is of special importance for paleontologists because it will cause preferential dissolution of aragonitic shells that are simultaneously replaced by silica precipitation, resulting in silicified fossils (chiefly of mollusks) and preserving the finest sculptural details (e.g., Kaim et al. 2008, 2009; Hybertsen and Kiel 2018; Hryniewicz et al. 2019).

These later diagenetic components are unique to ancient seep deposits and are unknown from their extant counterparts. Burial diagenetic pore fluids feature a chemistry different from that of seawater, and the seep deposit can be progressively isolated from marine and hydrocarbon-rich solutions (Campbell et al. 2002). Under these burial conditions, new phases and modification of existing ones can result in the dissolution of metastable minerals and their replacement with low-Mg calcite (cf. Bathurst 1975). Depending on the geological history of the area where a given ancient seep is located, the late diagenetic components differ in each deposit. For example, there are ancient seep carbonates which show very little (if any) late diagenetic carbonate. One such case is the latest Jurassic limestone boulders from Novaya Zemlya (Hryniewicz et al. 2015a), which are composed of microcrystalline

carbonate cementing fecal pellets, corrosion surfaces with or without associated pyrite, and banded cements lining the cavities. The remainder of the cavities is void, with no late diagenetic cements having been precipitated. Values of $\delta^{18}O$ in these seep carbonates range from −1.3‰ to 0.0‰ VPDB (with one outlier of −3.1‰ VPDB), which indeed indicates little diagenetic overprint. The geological area where the Novaya Zemlya boulders formed (this is unknown since all the boulders studied are erratics) has likely experienced little burial since the latest Jurassic. On the other end of the spectrum are seep deposits with complex late diagenetic histories and components (Fig. 3.10f). For example, Albian (Early Cretaceous) seeps from the Basque-Cantabrian Basin are filled with successive generations of calcite and dolomite cements, as well as pyrobitumen formed during burial involving rifting, emplacement of magmatic intrusions, petroleum generation and migration, and folding (Agirrezabala 2009; Jakubowicz et al. 2021). Deep burial and loading may also lead to pressure dissolution of seep carbonates, leaving characteristic pressure-solution seams reminiscent of those known from "normal" marine carbonates (e.g., Hryniewicz et al. 2021; cf. Łuczyński 2001). Epigenetic weathering during unroofing may result in oxidation of reduced compounds, such as pyrite, and formation of gypsum (Blouet et al. 2017).

3.6 Concluding Remarks and Future Directions

Recognition of ancient seep deposits is based on geochemical, faunal, geological, and petrographic criteria (Campbell 2006). Geochemical criteria, specifically low $\delta^{13}C$ and presence of ^{13}C-depleted lipid biomarkers typical of AOM-mediating microbial consortia, are undoubtedly most decisive for recognition of seep-related carbonates in the fossil record. Faunal criteria, i.e., the identification of fossil seep-obligate fauna, such as vesicomyid bivalves or abyssochryssoid gastropods, are also important for identification of a given ancient carbonate as seep-related. However, there are cases when the most straightforward criteria (geochemical and faunal) are unavailable and a seep origin of the carbonate has to be ascertained mostly on petrographic grounds. For example, carbonates from the latest Silurian El-Borj seep deposit in Morocco have relatively high $\delta^{13}C$ signatures (not lower than −6‰ VPDB) and thus are not low enough to be easily classified as seep-related purely on geochemical grounds. Faunal criteria are also not decisive, since the only fossil known from this deposit is the atrypid gastropod *Septatrypa lantenoisi*, which does not belong to a group associated with ancient seep deposits. Yet, the presence of banded cements typical for seep deposits led Jakubowicz et al. (2017) to tie the origin of the El-Borj deposit to methane seepage and to explain the anomalously heavy carbon isotope composition of the carbonates to the positive $\delta^{13}C$ Ludfordian excursion, which shifted seawater and seep carbonate $\delta^{13}C$ toward higher values (Jakubowicz et al. 2017). This interpretation was further strengthened by the discovery of a species of the seep-restricted modiomorphid bivalve *Ataviaconcha* at El-Borj, which was previously known only from a Middle Devonian Hollard Mound

seep deposit (Hryniewicz et al. 2017). Hence, in spite of the multitude of geochemical approaches available in the twenty-first century, petrographic methods are still an important part of the diagnosis of ancient seep deposits.

Most seep carbonates are known from the Cenozoic and Cretaceous, with Jurassic and especially older deposits much less common. For example, there are only nine Jurassic, three Triassic, two Carboniferous, one Devonian, and one Silurian unequivocal seep deposit known. It is currently unknown whether this pattern is an expression of the "pull of the *recent*" phenomenon (Raup 1979) or if there are other explanations. It has been suggested that substrate bio-irrigation by marine fauna (e.g., chemosymbiotic bivalves and vestimentiferan tube worms) can enhance AOM and carbonate authigenesis at seeps (Luff et al. 2004). A consistent increase in the number of known seep carbonates from the Late Jurassic/Early Cretaceous-age interval onward does indeed coincide with the colonization of seeps by infaunal lucinid and thyasirid bivalves, which are efficient bio-irrigators. Bio-irrigation takes place through burrows, and these (when preserved) are easily observed in macro- and microscopic samples of seep carbonates. Thus, establishing petrographic and geochemical criteria for bio-irrigation at ancient seeps is a step toward testing the hypothesis on faunal forcing of increased carbonate mineralization at seeps during the Meso- and Cenozoic.

There are no unequivocal seep deposits of Proterozoic, Cambrian or Ordovician age known. Further exploration and collecting may help discover such deposits and move the geological age of carbonate mineralization at seeps further back in time.

Acknowledgments I am very thankful to editors Andrzej Kaim (Institute of Paleobiology PAS, Poland), J. Kirk Cochran (Stony Brook University, New York, USA), and Neil H. Landman (American Museum of Natural History, New York, USA) for an opportunity to contribute to this book. I would like also to thank Andrzej Kaim for donating whole rock specimens and photos from various seep deposits around the world, which I used during the preparation of this chapter. Many fruitful discussions in the office and in the field with Kazutaka Amano (Joetsu University of Education, Joetsu, Japan), Michał Jakubowicz (Adam Mickiewicz University, Poznań, Poland), Robert G. Jenkins (Kanazawa University, Kanazawa, Japan), Andrzej Kaim, Steffen Kiel (Swedish Museum of Natural History, Stockholm, Sweden), and Crispin T.S. Little (University of Leeds, Leeds, UK) are sincerely acknowledged. Special thanks goes to referees J. Kirk Cochran and Jennifer Zwicker (University of Vienna, Vienna, Austria) for their thorough reviews which helped substantially improve this contribution.

References

Ager DV (1965) The adaptations of Mesozoic brachiopods to different environments. Palaeogeog Palaeoclimat Palaeoecol 1:143–172

Agirrezabala LM (2009) Mid-Cretaceous hydrothermal vents and authigenic carbonates in a transform margin, Basque-Cantabrian Basin (western Pyrenees): a multidisciplinary study. Sedimentology 56:969–996

Agirrezabala LM, Kiel S, Blumenberg M et al (2013) Outcrop analogues of pockmarks and associated methane-seep carbonates: a case study from the Lower Cretaceous (Albian) of the Basque-Cantabrian Basin, western Pyrenees. Palaeogeog Palaeoclimat Palaeoecol 390:94–115

Aissaoui DM (1985) Botryoidal aragonite and its diagenesis. Sedimentology 32:345–361
Aissaoui DM (1988) Magnesian calcite cements and their diagenesis: dissolution and dolomitization, Mururoa Atoll. Sedimentology 35:821–841
Allison PA, Hasselbo SP, Brett CE (2008) Methane seeps on Early Jurassic dysoxic seafloor. Palaeogeog Palaeoclimat Palaeoecol 270:230–238
Aloisi G, Pierre C, Rouchy J-M et al (2000) Methane-related authigenic carbonates of eastern Mediterranean Sea mud volcanoes and their possible relation to gas hydrate destabilization. Earth Planet Sci Lett 184:321–338
Amano K, Jenkins RG, Sako Y et al (2013) A Paleogene deep-sea methane-seep community from Honshu, Japan. Palaeogeog Palaeoclimat Palaeoecol 387:126–133
Baker PA, Kastner M (1981) Constraints on the formation of sedimentary dolomite. Science 213:214–216
Barbieri R, Cavalazzi B (2005) Microbial fabrics from Neogene cold-seep carbonates, northern Apennine, Italy. Palaeogeog Palaeoclimat Palaeoecol 227:143–155
Barbieri R, Ori GG, Cavalazzi B (2005) A Silurian cold-seep ecosystem from the Middle Atlas, Morocco. Palaios 19:527–542
Bathurst RCG (1975) Carbonate sediments and their diagenesis. Elsevier, Amsterdam
Berti M, Cuzzani MG, Landuzzi A et al (1994) Hydrocarbon-derived imprints in olistostromes of the Early Sarrevallian Marnoso-arenacea Formation, Romagna Appenines (northern Italy). Geo-Mar Lett 14:192–200
Blouet J-P, Imbert P, Fourbet A (2017) Mechanisms of biogenic gas formation revealed by seep carbonate paragenesis, Panoche Hills, California. Am Assoc Pet Geol Bull 101:1309–1340
Boetius A, Suess E (2004) Hydrate Ridge: a natural laboratory for the study of microbial life fueled by methane from near-surface gas hydrates. Chem Geol 205:291–310
Boetius A, Ravenschlag K, Schubert CJ et al (2000) A marine microbial consortium apparently mediating anaerobic oxidation of methane. Nature 407:623–626
Bohrmann G, Greinert J, Suess E et al (1998) Authigenic carbonates from the Cascadia subduction zone and their relation to gas hydrate stability. Geology 26:647–650
Bojanowski MJ (2007) Oligocene cold-seep carbonates from the Carpathians and their inferred relation to gas hydrates. Facies 53:347–360
Buggisch W, Krumm S (2005) Palaeozoic cold seep carbonates from Europe and North Africa—an integrated isotopic and geochemical approach. Facies 51:566–583
Campbell KA (2006) Hydrocarbon seep and hydrothermal vent palaeoenvironments and paleontology: past developments and future research directions. Palaeogeog Palaeoclimat Palaeoecol 232:362–407
Campbell KA, Bottjer D (1993) Fossil cold seeps. Natl Geogr Res Explor 9:326–343
Campbell KA, Bottjer D (1995) Brachiopods and chemosymbiotic bivalves in Phanerozoic hydrothermal vent and cold seep environments. Geology 23:321–324
Campbell KA, Farmer JD, Des Marais D (2002) Ancient hydrocarbon seeps from Mesozoic convergent margin of California: carbonate geochemistry, fluids and palaeonenvironments. Geofluids 2:63–94
Campbell KA, Francis DA, Collins M et al (2008) Hydrocarbon seep carbonates of a Miocene forearc (East Coast Basin), North Island, New Zealand. Sediment Geol 204:83–105
Carson B, Screaton EJ (1998) Fluid flow in accretionary prism: evidence for focused, time-variable discharge. Rev Geophys 36:329–351
Cochran JK, Landman NH, Jakubowicz M et al (this volume) Geochemistry of Cold Hydrocarbon Seeps: An Overview. In: Kaim A, Cochran JK, Landman NH (eds) Ancient hydrocarbon seeps, Topics in geobiology, vol 50. Springer, Cham
Conti S, Fontana D (2007) Anatomy of seep carbonates: ancient examples from the Miocene of northern Apennines (Italy). Palaeogeog Palaeoclimat Palaeoecol 227:156–175
Conti S, Artoni A, Piola G (2007) Seep-carbonates in a thrust-related anticline at the leading edge of an orogenic wedge: the case of the middle–late Miocene Salsomaggiore Ridge (northern Apennines, Italy). Sediment Geol 199:233–251

Danner WR (1966) Limestone resources of western Washington. State Wash Div Mines Geol Bull 52:1–474

De Beaver E, Birgel D, Muchez P et al (2011) Fabric and formation of grapestone concretions within an unusual ancient methane seep system. Terra Nova 23:56–61

Diaz M, Eberli GP (2022) Microbial contribution to early marine cementation. Sedimentology 9:798 –822

Dupraz C, Reid PR, Braissant O et al (2009) Process of carbonate cementation in modern microbial mats. Earth Sci Rev 96:141–162

Duranti D, Mazzini A (2005) Large-scale hydrocarbon-driven sand injection in the Paleogene of the North Sea. Earth Planet Sci Lett 239:327–335

Feng D, Chen D, Roberts HH (2008) Sedimentary fabrics in the authigenic carbonates from Bush Hill: implications for the seabed fluid flow and its dynamic signature. Geofluids 8:301–310

Feng D, Chen D, Peckmann J et al (2010) Authigenic carbonates from methane seeps of the northern Congo fan: microbial formation mechanism. Mar Pet Geol 27:748–756

Flajs G, Vigener M, Keupp H et al (1995) Mud mounds: a polygenetic spectrum of fine-grained carbonate buildups. Facies 32:1–70

Flügel E (2004) Microfacies of carbonate rocks: analysis, interpretation and application. Springer, Berlin

Gaillard C, Rio M, Rolin Y et al (1992) Fossil chemosynthetic communities related to vents or seeps in sedimentary basins: the pseudobioherms of southeastern France compared to other world examples. Palaios 7:451–465

Gill FL, Harding IC, Little CTS et al (2005) Palaeogene and Neogene cold-seep communities in Barbados, Trinidad and Venezuela: an overview. Palaeogeog Palaeoclimat Palaeoecol 227:191–209

Goedert JL, Benham SR (2003) Biogeochemical processes at ancient methane seeps: the Bear River site in southwestern Washington. In: Swanson TW (ed) Western Cordillera and adjacent areas, vol 4. Geological Society of America Field Guide, Boulder, pp 201–208

Goedert JL, Peckmann J, Reitner J (2000) Worm tubes in an allochtonous cold-seep carbonate from lower Oligocene rocks in western Washington. J Paleontol 74:992–999

Gómez-Pérez I (2003) An early Jurassic deep-water stromatolitic bioherm related to possible methane seepage (Los Molles Formation, Neuquén, Argentina). Palaeogeog Palaeoclimat Palaeoecol 201:21–49

Grammer GM, Ginsburg RN, Swart PK et al (1993) Rapid growth rates of syndepositional marine aragonite cements in steep marginal slope deposits, Bahamas and Belize. J Sediment Petrol 63:983–989

Greinert J, Bohrmann G, Suess E (2001) Gas hydrate-associated carbonates and methane-venting at Hydrate Ridge: classification, distribution, and origin of authigenic lithologies. In: Paull CK, Dillon PW (eds) Natural gas hydrates: occurrence, distribution, and detection, Geophysical Monograph, vol 124, pp 99–113

Greinert J, Bohrmann G, Elvert M (2002) Stromatolitic fabric of authigenic carbonate crust: results of anaerobic methane oxidation at cold seeps in 4,850 m water depth. Int J Earth Sci 91:698–711

Haas A, Little CTS, Sahling H et al (2009) Mineralization of vestimentiferan tubes at methane seeps on the Congo deep-sea fan. Deep-Sea Res I 56:283–293

Haas A, Peckmann J, Elvert M et al (2010) Patterns of carbonate authigenesis at the Kouilou pockmarks on the Congo deep-sea fan. Mar Geol 268:129–136

Hagemann A, Leefmann T, Peckmann J et al (2013) Biomarkers from individual carbonate phases of an Oligocene cold-seep deposit, Washington State, USA. Lethaia 46:7–18

Hammer Ø, Nakrem HA, Little CTS et al (2011) Hydrocarbon seeps from close to the Jurassic–Cretaceous boundary. Palaeogeog Palaeoclimat Palaeoecol 306:15–26

Hickman CS (2015) Paleogene marine bivalves of the deep-water Keasey Formation in Oregon, part III: the heteroconchs. PaleoBios 32:1–44

Hikida Y, Suzuki S, Togo Y et al (2003) An exceptionally well-preserved fossil seep community from the Cretaceous Yezo Group in the Nakagawa area, Hokkaido, northern Japan. Paleontol Res 7:329–342
Himmler T, Brinkmann T, Bohrmann G et al (2011) Corrosion patterns of seep carbonates from the eastern Mediterranean Sea. Terra Nova 23:206–212
Himmler T, Birgel D, Bayon G et al (2015) Formation of seep carbonates along the Makran convergent margin, northern Arabian Sea and a molecular and isotopic approach to constrain the carbon isotopic composition of parent methane. Chem Geol 415:102–117
Himmler T, Bayon G, Wangner D et al (2016) Seep-carbonate lamination controlled by cyclic particle flux. Sci Rep 6:37439
Himmler T, Smrzka D, Zwicker J et al (2018) Stromatolites below the photic zone in the northern Arabian Sea formed by calcifying microbial mats. Geology 46:339–342
Hovland M (2002) On the self-sealing nature of marine seeps. Cont Shelf Res 22:2387–2394
Hovland M, Judd A (2007) Seabed fluid flow: the impact on biology, geology and the marine environment. Cambridge University Press, Cambridge
Hovland M, Svensen H (2006) Submarine pingoes: indicators of shallow gas hydrates in a pockmark at Nyegga, Norwegian Sea. Mar Geol 228:15–23
Hryniewicz K, Hammer Ø, Nakrem HA et al (2012) Microfacies of the Volgian–Ryazanian (Jurassic–Cretaceous) hydrocarbon seep carbonates from Sassenfjorden, central Spitsbergen, Svalbard. Norw J Geol 92:113–131
Hryniewicz K, Little CTS, Nakrem HA (2014) Bivalves from the latest Jurassic–earliest Cretaceous hydrocarbon seep carbonates from central Spitsbergen, Svalbard. Zootaxa 3859:1–66
Hryniewicz K, Hagström J, Hammer Ø et al (2015a) Late Jurassic–Early Cretaceous hydrocarbon seep boulders from Novaya Zemlya and their faunas. Palaeogeog Palaeoclimat Palaeoecol 436:231–244
Hryniewicz K, Nakrem HA, Hammer Ø et al (2015b) Palaeoecology of latest Jurassic–earliest Cretaceous hydrocarbon seep carbonates from Spitsbergen, Svalbard. Lethaia 48:353–374
Hryniewicz K, Bitner MA, Durska E et al (2016) Paleocene methane seep and wood-fall marine environments from Spitsbergen, Svalbard. Palaeogeog Palaeoclimat Palaeoecol 462:41–56
Hryniewicz K, Jakubowicz M, Belka Z et al (2017) New bivalves from the Middle Devonian methane seep in Morocco: the oldest record of repetitive shell morphologies among some seep bivalve molluscs. J Syst Palaeontol 15:19–41
Hryniewicz K, Amano K, Bitner MA et al (2019) A late Paleocene fauna from shallow-water chemosynthesis-based ecosystems, Spitsbergen, Svalbard. Acta Palaeontol Pol 64:101–141
Hryniewicz K, Miyajima Y, Amano K et al (2021) Formation, diagenesis and fauna from the Miocene Taishu Group of Tsushima (Japan). Geol Mag 158:964–984
Hybertsen F, Kiel S (2018) A middle Eocene seep deposit with silicified fauna from the Humptulips Formation in western Washington State, USA. Acta Palaeontol Pol 63:751–758
Jakubowicz M, Hryniewicz K, Belka Z (2017) Mass occurrence of seep-specific bivalves in the oldest-known cold seep metazoan community. Sci Rep 7:14292
Jakubowicz M, Agirrezabala L, Dopieralska J et al (2021) The role of magmatism in hydrocarbon generation in sedimented rifts: a Nd isotope perspective from mid-Cretaceous methane-seep deposits of the Basque-Cantabrian Basin, Spain. Geochim Cosmochim Acta 303:223–248
Jenkins RG, Kaim A, Hikida Y (2007) Methane-flux-dependent lateral faunal changes in the Late Cretaceous chemosymbiotic assemblage from the Nakagawa area of Hokkaido, Japan. Geobiology 5:127–139
Jenkins RG, Kaim A, Little CTS et al (2013) Worldwide distribution of the modiomorphid bivalve genus *Caspiconcha* in late Mesozoic hydrocarbon seeps. Acta Palaeontol Pol 58:357–382
Jørgensen NO (1989) Holocene methane-derived, dolomite-cemented sandstone pillars from the Kattegat, Denmark. Mar Geol 88:71–81
Joye SB (2020) The geology and biogeochemistry of hydrocarbon seeps. Ann Rev Earth Planet Sci 48:205–231

Kaim A, Jenkins RG, Warén A (2008) Provannid and provannid-like gastropods from Late Cretaceous cold seeps of Hokkaido (Japan) and the fossil record of Provannidae. Zool J Linn Soc 154:421–436

Kaim A, Jenkins RG, Hikida Y (2009) Gastropods from Late Cretaceous Omagari and Yasukawa hydrocarbon seep deposits in the Nakagawa area, Hokkaido, Japan. Acta Palaeontol Pol 54:463–490

Kaim A, Skupien P, Jenkins RG (2013) A new Lower Cretaceous hydrocarbon seep locality from the Czech Carpathians and its fauna. Palaeogeog Palaeoclimat Palaeoecol 390:42–51

Kauffman EG, Arthur MA, Howe B et al (1996) Widespread venting of methane-rich fluids in Late Cretaceous (Campanian) submarine springs (Tepee Buttes), Western Interior Seaway, U.S.A. Geology 24:799–802

Kelly SRA, Ditchfield PW, Doubleday PA et al (1995) An Upper Jurassic methane-seep limestone from the Fossil Bluff Group Forearc Basin of Alexander Island, Antarctica. J Sediment Res A 65:274–282

Kelly SRA, Blanc E, Price SP et al (2000) Early Cretaceous giant bivalves from seep-relate limestone mounds, Wollaston Forland, northeast Greenland. In: Harper EM, Taylor JD, Crame JA (eds) The evolutionary biology of the Bivalvia. Geological Society of London, London, pp 227–246

Kiel S (2010) An Eldorado for palaeontologists: the Cenozoic seeps of western Washington State, USA. In: Kiel S (ed) The vent and seep biota. Springer, Heidelberg, pp 433–448

Kiel S, Peckmann J (2007) Chemosymbiotic bivalves and stable carbon isotopes indicate hydrocarbon seepage and four unusual Cenozoic fossil localities. Lethaia 40:345–357

Kiel S, Peckmann J (2008) Paleoecology and evolutionary significance of an Early Cretaceous *Peregrinella*-dominated hydrocarbon-seep deposit on the Crimean Peninsula. Palaios 23:751–759

Kiel S, Birgel D, Campbell KA et al (2013) Cretaceous methane-seep deposits from New Zealand and their fauna. Palaeogeog Palaeoclimat Palaeoecol 390:17–34

Kiel S, Glodny J, Birgel D et al (2014a) The paleoecology, habitats, and stratigraphic range of the enigmatic Cretaceous brachiopod *Peregrinella*. PLoS One 9(10):e109260

Kiel S, Hansen C, Nitzsche KN et al (2014b) Using $^{87}Sr/^{86}Sr$ to date fossil methane seep deposits: methodological requirements and an example for the Great Valley Group, California. J Geol 122:353–366

Kuechler RR, Birgel D, Kiel S et al (2012) Miocene methane-derived authigenic carbonates from southwestern Washington, USA and a model for silification at seeps. Lethaia 45:259–273

Landman NH, Cochran JK, Larson NL et al (2012) Methane seeps as ammonite habitats in the U.S. Western Interior Seaway revealed by isotopic analyses of well-preserved shell material. Geology 40:507–510

Landman NH, Cochran KJ, Brezina J et al (this volume) Methane seeps in the Late Cretaceous Western Interior Seaway. In: Kaim A, Cochran JK, Landman NH (eds) Ancient hydrocarbon seeps, Topics in geobiology, vol 50. Springer, Cham

Leefmann T, Bauermeister J, Kronz A et al (2008) Miniaturized biosignature analysis reveals implications for the formation of cold seep carbonates at Hydrate Ridge (off Oregon, USA). Biogeosciences 5:731–738

Levin LA (2005) Ecology of cold seep sediments: interactions of fauna with flow, chemistry and microbes. Oceanogr Mar Biol Annu Rev 43:1–46

Little CTS, Birgel D, Boyce AJ et al (2015) Late Cretaceous (Maastrichtian) shallow water hydrocarbon seeps from Snow Hill and Seymour Islands, James Ross Basin, Antarctica. Palaeogeog Palaeoclimat Palaeoecol 418:213–228

Lu Y, Xiaming S, Xu H et al (2018) Formation of dolomite catalyzed by sulfate-driven anaerobic oxidation of methane: mineralogical and geochemical evidence from the northern South China Sea. Am Mineral 103:720–734

Łuczyński P (2001) Pressure-solution and chemical compaction of condensed Middle Jurassic deposits, High-Tatric Series, Tatra Mountains. Geol Carpathica 52:91–102

Luff R, Wallmann K (2003) Fluid flow, methane fluxes, carbonate precipitation and biogeochemical turnover in gas hydrate-bearing sediments at Hydrate Ridge, Cascadia Margin: numerical modeling and mass balance. Geochim Cosmochim Acta 67:3403–3421

Luff R, Wallmann K, Aloisi G (2004) Numerical modelling of carbonate crust formation at cold vent sites: significance for fluid and methane budgets and chemosynthetic biological communities. Earth Planet Sci Lett 221:337–357

Luff R, Greinert J, Wallmann K et al (2005) Simulation of long-term feedbacks from authigenic carbonate crust formation at cold vent sites. Chem Geol 216:157–174

Magalhães V, Pinheiro LM, Ivanov MK et al (2012) Formation process of methane-derived authigenic carbonates from the Gulf of Cadiz. Sediment Geol 243(244):155–168

Matsumoto R (1990) Vuggy carbonate crust formed by hydrocarbon seepage on the continental shelf of Baffin Island, northeast Canada. Geochem J 24:143–158

Mazzini A, Ivanov MK, Parnell J et al (2004) Methane-related authigenic carbonates from the Black Sea: geochemical characterization and relation to seeping fluids. Mar Geol 212:153–181

Mazzini A, Aloisi G, Akhmanov GG et al (2005) Integrated petrographic and geochemical record of hydrocarbon seepage on Vøring Plateau. J Geol Soc London 162:815–827

Mazzini A, Svensen H, Hovland M et al (2006) Comparisons and implications from strikingly different authigenic carbonates in a Nyegga complex pockmark, G11, Norwegian Sea. Mar Geol 231:89–102

Meehan KC, Landman NH (2016) Faunal associations in cold-methane seep deposit from the Upper Cretaceous Pierre Shale, South Dakota. Palaios 31:291–301

Miyajima Y, Jenkins JG (this volume) Biomarkers in Ancient Hydrocarbon-Seep Carbonates. In: Kaim A, Cochran JK, Landman NH (eds) Ancient hydrocarbon seeps, Topics in geobiology, vol 50. Springer, Cham

Miyajima Y, Watanabe Y, Yanagisawa Y et al (2016) A late Miocene methane seep deposit bearing methane-trapping silica minerals at Joetsu, central Japan. Palaeogeog Palaeoclimat Palaeoecol 455:1–15

Monty CLV, Bosence DWJ, Bridges PH et al (1995) Carbonate mud-mounds: their origin and evolution. Int Assoc Sedimentologists Spec Publ 23:11–48

Natalicchio M, Peckmann J, Birgel D et al (2015) Seep deposits from northern Istria, Croatia: a first glimpse into the Eocene seep fauna of the Tethys region. Geol Mag 152:444–459

Nesbitt EA, Martin RA, Campbell KA (2013) New records of Oligocene diffuse hydrocarbon seeps, northern Cascadia margin. Palaeogeog Palaeoclimat Palaeoecol 390:116–129

Nobuhara T (2016) Mass occurrence of the enigmatic gastropod *Elmira* in the Late Cretaceous Sada Limestone seep deposit in southwestern Shikoku, Japan. PalZ 90:701–722

O'Reilly SS, Hryniewicz K, Little CTS et al (2014) Shallow water methane-derived authigenic carbonate at the Codling Fault Zone, western Irish Sea. Mar Geol 357:139–150

Pape T, Geprägs P, Hammerschmidt S et al (2014) Hydrocarbon seepage and its sources at mud volcanoes of the Kumano Forearc Basin, Nankai Trough subduction zone. Geochem Geophys Geosyst 15:2180–2194

Pearson MJ, Grosjean E, Nelson CS et al (2010) Tubular concretions in New Zealand petroliferous basins: lipid biomarker evidence for mineralization around proposed Miocene hydrocarbon seep conduits. J Pet Geol 33:205–220

Peckmann J, Thiel V (2004) Carbon cycling and ancient methane seeps. Chem Geol 205:443–467

Peckmann J, Little CTS, Gill F et al (2005) Worm tube fossils from the Hollard Mound hydrocarbon-seep deposit, Middle Devonian, Morocco: Palaeozoic seep-related vestimentiferans? Palaeogeogr Palaeoclimatol Palaeoecol 227:242–257

Peckmann J, Thiel V, Michaelis W et al (1999a) Cold seep deposits of Beauvoisin (Oxfordian; southeastern France) and Marmorito (Miocene, northern Italy): microbially induced authigenic carbonates. Int J Earth Sci 88:60–75

Peckmann J, Walliser O, Riegel W et al (1999b) Signatures of hydrocarbon venting in the Middle Devonian carbonate mound (Hollard Mound) at the Hamar Laghdad (Morocco). Facies 40:281–296

Peckmann J, Reimer A, Luth U et al (2001) Methane-derived carbonates and authigenic pyrite from the northwestern Black Sea. Mar Geol 177:129–150
Peckmann J, Goedert JL, Thiel V et al (2002) A comprehensive approach to the study of methane-seep deposits from the Lincoln Creek Formation, western Washington State, USA. Sedimentology 49:855–873
Peckmann J, Goedert JL, Heinrichs T et al (2003) A late Eocene 'Whiskey Creek' methane seep deposit (western Washington State): part II, petrology, stable isotopes, and biogeochemistry. Facies 48:241–254
Peckmann J, Campbell KA, Walliser OH et al (2007) A Late Devonian hydrocarbon-seep deposit dominated by dimerelloid brachiopods, Morocco. Palaios 22:114–122
Peckmann J, Kiel S, Sandy MR et al (2011) Mass occurrence of the brachiopod *Halorella* in Late Triassic methane-seep deposits, eastern Oregon. J Geol 119:207–220
Perez-Garcia C, Feseker T, Mienert J et al (2009) The Håkon Mosby mud volcano: 330000 years of focused fluid flow activity at the SW Barents Sea slope. Mar Geol 262:105–115
Pierre C, Fouquet Y (2007) Authigenic carbonates from methane seeps of the Congo deep-sea fan. Geo-Mar Lett 27:249–257
Raup DM (1979) Biases in the fossil record of species and genera. Bull Carnegie Mus Nat His 13:85–91
Reitner J, Peckmann J, Blumenberg M et al (2005a) Concretionary methane-seep carbonates and associated microbial communities in Black Sea sediments. Palaeogeog Palaeoclimat Palaeoecol 227:18–30
Reitner J, Peckmann J, Reimer A et al (2005b) Methane-derived carbonate buildups and associated microbial communities at cold seeps on the lower Crimean shelf (Black Sea). Facies 51:66–79
Ritger S, Carson B, Suess E (1987) Methane-derived authigenic carbonates formed by subduction-induced pore-water expulsion along the Oregon/Washington margin. Geol Soc Am Bull 98:147–156
Riding RE, Awramik SM (2000) Microbial sediments. Springer, Heidelberg
Römer M, Sahling H, Pape T et al (2012) Quantification of gas bubble emissions from submarine hydrocarbon seeps at the Makran continental margin (offshore Pakistan). J Geophys Res 117:C10015
Ross DJ (1991) Botryoidal high-magnesium calcite marine cements from the Upper Cretaceous of the Mediterranean Region. J Sediment Petrol 61:349–353
Sahling H, Rickert D, Lee RW et al (2002) Macrofaunal community structure and sulfide flux at gas hydrate deposits from the Cascadia convergent margin, NE Pacific. Mar Ecol Prog Ser 231:121–138
Sandy MR (2010) Brachiopods from ancient hydrocarbon seeps and hydrothermal vents. In: Kiel S (ed) The vent and seep biota. Springer, Heidelberg, pp 279–314
Savard MM, Beauchamp B, Veizer J (1996) Significance of aragonite cements around Cretaceous marine methane seeps. J Sediment Res 66:430–438
Shapiro RS (2000) A comment on the systematic confusion of thrombolites. Palaios 15:166–169
Sibuet M, Olu K (1998) Biogeography, biodiversity and fluid dependence of deep-sea cold-seep communities at active and passive margins. Deep-Sea Res Part II 45:517–567
Smrzka D, Kraemer SM, Zwicker J et al (2015) Constraining silica diagenesis in methane-seep deposits. Palaeogeog Palaeoclimat Palaeoecol 420:13–26
Smrzka D, Zwicker J, Kolonic S et al (2017) Methane seepage in a Cretaceous greenhouse world recorded by an unusual carbonate deposit from the Tarfaya Basin, Morocco. Depositional Rec 3:4–37
Smrzka D, Zwicker J, Misch D et al (2019) Oil seepage and carbonate formation: a case study from the southern Gulf of Mexico. Sedimentology 66:2318–2353
Smrzka D, Zwicker J, Lu Y et al (2021) Trace element distribution in methane-seep carbonates: the role of mineralogy and dissolved sulfide. Chem Geol 580:120357
Stakes DS, Orange D, Paduan JB et al (1999) Cold seeps and authigenic carbonate formation in Monterey Bay, California. Mar Geol 159:93–109

Takeuchi R, Matsumoto R, Ogihara S et al (2007) Methane-induced dolomite 'chimneys' on the Kuroshima Knoll, Ryukyu Islands, Japan. J Geochem Explor 95:16–28

Teichert B, Eisenhauer A, Bohrmann G et al (2003) U/Th systematics and ages of authigenic carbonates from Hydrate Ridge, Cascadia Margin: records of fluid flow variations. Geochim Cosmochim Acta 67:3845–3857

Teichert B, Bohrmann G, Suess E (2005) Chemocherms on Hydrate Ridge—unique microbially-mediated carbonate build-ups growing into the water column. Palaeogeog Palaeoclimat Palaeoecol 227:67–85

Tong H, Feng D, Peckman J et al (2019) Environments favoring dolomite formation at cold seeps: a case study from the Gulf of Mexico. Chem Geol 518:9–18

Tsunogai U, Kosaka A, Nakayama N et al (2010) Origin and fate of deep-sea seeping methane bubbles at Kuroshima Knoll, Ryukyu forearc region, Japan. Geochem J 44:461–476

Van Dover CL, Aharon P, Bernhard JM et al (2002) Blake Ridge methane seeps: characterization of a soft-sediment, chemosynthetically based ecosystem. Deep-Sea Res I 50:281–300

Vanneste H, Kastner M, James RH et al (2012) Authigenic carbonates from the Darwin Mud Volcano, Gulf of Cadiz: a record of palaeo-seepage of hydrocarbon-bearing fluids. Chem Geol 300(301):24–39

Vinn O, Kupriyanova E, Kiel S (2013) Serpulids (Annelida, Polychaeta) at Cretaceous to modern hydrocarbon seeps: ecological and evolutionary patters. Palaeogeog Palaeoclimat Palaeoecol 390:35–41

Vinn O, Hryniewicz K, Little CTS et al (2014) A boreal seprulid fauna from Volgian–Ryazanian (latest Jurassic–earliest Cretaceous) shelf sediments and hydrocarbon seeps from Svalbard. Geodiversitas 36:527–540

Webb KE, Barnes DKA, Planke S (2009) Pockmarks: refugees for marine benthic biodiversity. Limnol Oceanogr 54:1776–1788

Wiese F, Kiel S, Pack A et al (2015) The beast burrowed, the fluid followed—crustacean burrows as methane conduits. Mar Pet Geol 66:631–640

Zwicker J, Smrzka D, Gier S et al (2015) Mineralized conduits are part of the uppermost plumbing system of Oligocene methane-seep deposits, Washington State (USA). Mar Pet Geol 66:616–630

Zwicker J, Smrzka D, Himmler T et al (2018) Rare earth elements as tracers for microbial activity and early diagenesis: a new perspective for carbonate cements of ancient methane-seep deposits. Chem Geol 501:77–85

Zwicker J, Smrzka D, Steindl FR et al (2020) Mineral authigenesis within chemosynthetic microbial mats: coated grain formation and phosphogenesis at Cretaceous hydrocarbon seep, New Zealand. Depositional Rec 7:294–310